NASA TECHNICAL REPORT

NASA TR R-383

c. 1

LOAN COPY: RETURN
AFWL (DOUL)
KIRTLAND AFB, N.

TECH LIBRARY KAFB, NM
0068458

NASA TR R-383

FUNDAMENTAL MECHANISMS OF TENSILE FRACTURE IN ALUMINUM SHEET UNIDIRECTIONALLY REINFORCED WITH BORON FILAMENT

by Harvey W. Herring

Langley Research Center
Hampton, Va. 23365

NATIONAL AERONAUTICS AND SPACE ADMINISTRATION • WASHINGTON, D. C. • APRIL 1972

TECH LIBRARY KAFB, NM

0068458

1. Report No. NASA TR R-383	2. Government Accession No.	3. Recipient's Catalog No.
4. Title and Subtitle FUNDAMENTAL MECHANISMS OF TENSILE FRACTURE IN ALUMINUM SHEET UNIDIRECTIONALLY REINFORCED WITH BORON FILAMENT		5. Report Date April 1972
		6. Performing Organization Code
7. Author(s) Harvey W. Herring		8. Performing Organization Report No. L-8137
9. Performing Organization Name and Address NASA Langley Research Center Hampton, Va. 23365		10. Work Unit No. 134-03-23-01
		11. Contract or Grant No.
12. Sponsoring Agency Name and Address National Aeronautics and Space Administration Washington, D.C. 20546		13. Type of Report and Period Covered Technical Report
		14. Sponsoring Agency Code
15. Supplementary Notes		

16. Abstract

Results are presented from an experimental study of the tensile-fracture process in aluminum sheet unidirectionally reinforced with boron filament. The tensile strength of the material is severely limited by a noncumulative fracture mechanism which involves the initiation and sustenance of a chain reaction of filament fractures at a relatively low stress level. Matrix fracture follows in a completely ductile manner. The minimum filament stress for initiation of the fracture mechanism is shown to be approximately 1.17 GN/m^2 (170 ksi), and appears to be independent of filament diameter, number of filament layers, and the strength of the filament-matrix bond. All the commonly observed features of tensile fracture surfaces are explained in terms of the observed noncumulative fracture mechanism.

17. Key Words (Suggested by Author(s)) Metal-matrix composites Fracture	18. Distribution Statement Unclassified – Unlimited

19. Security Classif. (of this report) Unclassified	20. Security Classif. (of this page) Unclassified	21. No. of Pages 80	22. Price* $3.00

*For sale by the National Technical Information Service, Springfield, Virginia 22151

FUNDAMENTAL MECHANISMS OF TENSILE FRACTURE IN ALUMINUM SHEET UNIDIRECTIONALLY REINFORCED WITH BORON FILAMENT

By Harvey W. Herring
Langley Research Center

SUMMARY

Results are presented from an experimental research effort to gain a more complete understanding of the mechanisms of tensile fracture in composite sheet of aluminum unidirectionally reinforced with boron filament (B-Al). By varying the degree of filament degradation resulting from fabrication, composite specimens were produced which failed in tension by the cumulative mode, the noncumulative mode, or by any desired combination of the two modes. In the cumulative mode, fracture of a single filament influenced the subsequent fracture of only its few nearer neighbors. Cumulative fracture occurred slowly over a range of tensile load. Noncumulative fracture occurred at a constant load when failure of a single filament caused all the remaining filaments in the composite to break. The noncumulative mode resulted in nearly instantaneous composite fracture and imposed a severe limitation on the tensile strength of the material.

Radiographic and acoustic-emission techniques were combined to identify and describe physically a previously unrecognized fundamental fracture mechanism which was responsible for the noncumulative mode. The mechanism involved the initiation and sustenance of a chain reaction of filament fractures at a relatively low stress level followed by ductile fracture of the matrix. The minimum average filament stress required for initiation of the noncumulative mechanism was shown to be approximately 1.17 GN/m^2 (170 ksi), and, within the limited ranges investigated, appeared to be independent of filament diameter, number of filament layers, strength of interfacial bonds, and the identity of the matrix alloy.

A comprehensive analysis of tensile fracture surfaces revealed that characteristic features of the surfaces were determined by the mode of fracture. The characteristic features were categorized and related to the responsible fracture mechanism in such a way that subsequent fractographic analyses of B-Al tensile failures should be facilitated by direct comparison with the results of this investigation.

Tests of specimens which contained flaws in the form of internally broken filaments revealed that a relatively large proportion (up to 20 percent) of the filaments in a given specimen could be broken, and yet fracture of that specimen would invariably take place through a region remote from the preexisting breaks. Local stress concentrations resulting from internal filament breaks were apparently alleviated by matrix plasticity.

INTRODUCTION

Based on considerations of density, stiffness, and compressive strength, a composite of aluminum sheet unidirectionally reinforced with boron filament (B-Al) is regarded as a potentially useful material for advanced aerospace applications. The material offers two significant advantages over composites with resinous matrices. First, B-Al can perform effectively at temperatures up to 700 K (800° F) compared with a maximum of about 450 K (350° F) for boron-filament-reinforced epoxy. Second, the increased shear and transverse stiffnesses of the aluminum matrix allow unidirectionally reinforced B-Al to resist buckling loads effectively. In resinous-matrix composites, a comparable capability for withstanding buckling usually requires a more complicated multidirectional arrangement of filaments.

A perplexing problem associated with B-Al composite has been its disappointingly low tensile strength, with tensile failures frequently being observed at an average filament stress less than one-half the strength of the virgin filament used in fabrication of the composite. A recent investigation at the Langley Research Center (ref. 1) has shown that one commerically available B-Al composite, used in a structural element with sufficient support to prevent buckling, could routinely withstand compressive stresses on the order of 1.55 GN/m^2 (225 ksi) without failure. However, the tensile strength exhibited by the very same material, only 0.69 GN/m^2 (100 ksi), suggests that ultimate strength in tension was being regulated by a fracture mechanism which became operative at a relatively low stress level.

The problem of tensile fracture in composites containing parallel brittle filaments was analyzed by Zweben and Rosen (refs. 2, 3, and 4) in a series of recent papers. Zweben, in particular (ref. 2), described two fundamental fracture modes. One of them, the cumulative mode, was characterized by the gradual accumulation of a considerable number of individual filament breaks in advance of total composite fracture.

The cumulative mode can occur when filaments break under the influence of stress concentrations resulting from their previously broken neighbors, or when filaments break in scattered locations according to their individual load-bearing capabilities. Ultimate failure of the composite occurs instantaneously when the cross-sectional area of unbroken filaments becomes too small to withstand the increasing load.

The second fracture mode did not involve a significant number of individual filament breaks prior to composite fracture, and was referred to as the noncumulative mode. The actual mechanism of noncumulative fracture was not specified but was assumed to precipitate from the fracture of only a few of the weaker filaments in the composite.

The cumulative fracture mode was observed by Rosen (ref. 5) in the tensile failure of glass-filament-reinforced epoxy composites. The noncumulative mode was observed

by Mullin and his coworkers (refs. 6 and 7) in the failure of boron-epoxy and graphite-epoxy composites. In the work of Mullin et al., noncumulative fracture occurred in some composites when one of the first filaments to break initiated a matrix crack which propagated through both filaments and matrix to cause rapid, complete failure of the composite.

Most unidirectional composites of practical significance undergo tensile failure by a combination of the two modes proposed by Zweben. As load is increased, the weaker filaments break cumulatively, but above some threshold value of average filament stress, a noncumulative mechanism becomes operative to cause catastrophic fracture. The physical nature of the noncumulative mechanism depends on the local response of the matrix and the filament-matrix interfacial bond to the sudden release of elastic strain energy by a breaking filament. If the matrix responds by cracking, ultimate composite strength can possibly be improved by toughening the matrix, or by creating internal energy sinks to absorb a portion of the energy pulse. The strength increase would result from a broadening of the stress range over which cumulative fracture may occur, and a corresponding postponement of the disastrous noncumulative mode.

Mullin et al. were able to exercise control over the fracture process for boron-epoxy and graphite-epoxy composites by decreasing the crack sensitivity of the epoxy, and by adjusting the filament-matrix interfacial bond strength to allow energy absorption by a small amount of debonding near the newly formed ends of a broken filament. He was able to produce composites which failed cumulatively, noncumulatively, and by combinations of the two modes.

In this paper, results are presented from an experimental research effort to gain a more complete understanding of tensile fracture in unidirectionally reinforced B-Al composite sheet. By varying the degree of filament degradation resulting from fabrication, it was possible to produce composite specimens which failed in tension by the cumulative mode, the noncumulative mode, or by any desired combination of the two modes. Radiographic and acoustic-emission techniques were combined to identify and describe physically a previously unrecognized fracture mechanism which was responsible for the noncumulative mode. A threshold value of average filament stress below which the noncumulative mechanism was not operative was determined. Common features of tensile fracture surfaces were categorized and found to be compatible with the observed mechanism of fracture. The effects of internal stress concentrations in the form of previously broken filaments were investigated, and, to a limited extent, so were the effects of variations in matrix composition, filament spacing, and internal bond strengths.

The units used for the physical quantities defined in this paper are given both in the International System of Units (SI) (ref. 8) and in the U.S. Customary Units. The measurements and calculations were made in U.S. Customary Units. Factors relating the two systems of units are presented in appendix A.

MATERIALS AND SPECIMENS

Materials

The boron-aluminum (B-Al) composite used most extensively in this study was fabricated in small quantities at the Langley Research Center by a combined filament-winding and diffusion-bonding process. First-hand control was necessary to allow flexibility in the selection of fabrication parameters which affected the physical and mechanical properties of the composite. Unidirectionally reinforced sheet was produced which contained from one to five layers of either 0.099-mm-diameter (0.0039-in.) or 0.14-mm-diameter (0.0056-in.) boron filament spaced at 79 or 63 per cm (200 or 160 per in.), respectively, in a 1230 aluminum alloy matrix. The 1230 alloy was chosen because it was available in copious quantities at the Langley Research Center and because its purity (99.3 percent Al) would insure the production of clean, precipitate-free fracture surfaces.

The composite was consolidated by diffusion bonding under vacuum for 1 hour at temperatures ranging from 783 K (950° F) to 866 K (1100° F). Bonding pressures were varied between 62 MN/m^2 (9 ksi) and 103 MN/m^2 (15 ksi) in a deliberate attempt to influence the degree of filament degradation resulting from consolidation. In most cases, diffusion-bonding parameters were intentionally made severe to insure the production of generally well-bonded composite. No attempt was made to produce composite with optimum mechanical properties. The primary purpose of the research program was to gain a more complete understanding of the fundamental fracture characteristics of the material. Composite fabrication procedures were altered as necessary to serve that purpose. Details of the composite fabrication process are presented in appendix B.

Quantities of two different commerically produced B-Al composites were also included in the study. One material contained five layers of filament and was fabricated by filament winding and diffusion bonding 0.10-mm-diameter (0.0041-in.) silicon-carbide-coated boron filament and 2024 aluminum foil. The other was fabricated in a similar manner, but contained only one layer of 0.14-mm-diameter (0.0056-in.) boron filament in a 6061 aluminum alloy matrix. Specific fabrication parameters were not available from either manufacturer, but as is the general case for commercially available materials, filament-matrix and matrix-matrix bonds were relatively weak. That condition did not necessarily represent poor quality but resulted from reduced reactivity between silicon carbide and aluminum in the one case, and for both materials, the deliberate adjustment of fabrication parameters by the manufacturers to minimize filament degradation. The five-layer commercial material contained 48 percent filaments by volume. The monolayer composite contained 35 volume percent filaments.

Specimens

Composite tensile specimens, 1.27 cm wide (0.50 in.) with a gage length of 5.1 cm (2.0 in.), were cut from sheet material by electrical-discharge machining. A typical specimen is shown in figure 1 prior to testing. The specimens had straight edges and were cut so that load would be applied parallel to the filaments. Beveled fiber glass tabs with a nylon-flexibilized epoxy matrix were adhesively bonded to the specimen ends to insure a gradual transfer of load from the grips of the testing machine into the specimen.

A number of specimens were fabricated with internal flaws in the form of intentionally broken filaments. The flaws were created by placing a monolayer preform segment (see appendix B) under a low-power stereomicroscope and cutting (or crushing) the desired number of adjacent filaments with a scalpel. Filament breaks were located in the preform segment in such a way that after consolidation to produce a monolayer sheet, tensile specimens could be obtained with predetermined numbers of transverse breaks roughly centered in their gage sections.

Several cutting methods were tried for removing specimens from B-Al composite sheet, including shearing, diamond sawing, and electrical-discharge machining. The electrical-discharge method produced the smoothest edge and the least number of filament breaks near a machined edge. Figure 2 shows the typical appearance of a machined edge of a bilayer specimen. Only one filament is visible, and it has been neatly sliced parallel to its axis.

EXPERIMENTAL PROCEDURE

Composite Tests

Tensile testing.- The apparatus for composite tensile testing is represented schematically in figure 3. A specimen was mounted in a testing machine with sufficiently precise alinement to insure that tensile strains resulting from both in-plane and out-of-plane bending would be less than 2 percent of the total axial strain. For most of the tests, strain output was recorded from a single foil-type gage bonded to the center of one specimen surface. Strain was recorded autographically as a function of load. A few specimens with multiple strain gages were periodically tested to insure that alinement was being maintained. The strain rate was 0.002 per minute for all tests.

Acoustic monitoring.- A capacitance microphone was placed in the vicinity of the specimen to collect acoustic emissions during testing. Its output was amplified and routed through a loudspeaker so that sounds from filaments breaking, both individually and in groups, would be audible. The acoustic monitoring system was used to indicate the onset

of fracture, but was useful only when catastrophic fracture of the composite was preceded by at least a small number of filament failures. No attempt was made to record and analyze the acoustic-frequency spectrum associated with fracture.

Radiography.- A source of X-rays was placed so that a photographic plate on the opposite side of the specimen could be exposed to reveal interior details of the composite. Specimens were radiographed before loading, under load, and after failure in an attempt to establish the sequence of events involved in the fracture process. Kodak high-resolution plates were exposed for 10 to 15 minutes at an X-ray tube voltage of 100 kV. A short exposure time was desirable because of the large number of specimens involved in the program, and also because of the difficulty in maintaining a constant load on a specimen for long periods of time. Specimens in which ultimate fracture was preceded by cumulative breaking of filaments as a function of time could not be radiographed successfully at high loads because of the exposure time required.

Photography.- Photographs of the radiographic images were taken at magnifications up to $\times 550$ on Kodak metallographic plates. A bench metallograph was used with light transmitted through the plate containing the radiographic image. Matching fracture surfaces were observed and photographed on Polaroid film with the Cambridge Stereoscan scanning electron microscope. The B-Al composite was sufficiently conductive to obviate coating. No special techniques were required.

Fracture arrest.- In order to study the noncumulative mechanism of fracture, it was necessary to be able to stop the fracture process short of complete specimen failure. For most specimens tested, fracture, once initiated, was extremely rapid. Arresting a crack by load relaxation was a trial-and-error process which resulted in many fracture surfaces, but few arrested cracks. Nevertheless, that method was successful in a sufficient number of instances. In some specimens, alinement was accurate enough for two cracks to begin simultaneously at different locations. One crack would invariably result in separation of the specimen, and the other would be arrested for further study.

Filament Tensile Tests

A quantity of B-Al composite sheet having unique fabrication parameters was referred to as a batch. For at least one tensile specimen from each batch, the matrix was leached out in a warm sodium hydroxide solution, and the reclaimed filaments were tested individually. Tensile-strength distributions for filaments contained within each batch were thus determined. Gage length was 5.1 cm (2.0 in.) and strain rate was 0.002 per minute, the same as for the composite specimens. Filaments were gripped for testing by bonding their ends to grooved metal tabs with sealing wax according to the method described in reference 9.

RESULTS AND DISCUSSION

Most of the B-Al sheet material used in this study was well bonded. A strong diffusion bond had been achieved between foil layers during consolidation, and a chemical bond had been developed between the boron filaments and the aluminum matrix. The tensile failure mode for well-bonded composite was generally noncumulative provided the filaments had not been too severly degraded during consolidation. Ultimate failure of the composite was preceded by very few, if any, individual filament breaks. By adjusting the pressure and temperature involved in consolidation of the composite, however, it was possible to vary the fracture mode. Fracture could be made noncumulative, cumulative, or partially cumulative as desired.

The noncumulative mode will be discussed first and most extensively because the mechanism involved was the limiting factor in the failure of nearly all the specimens tested in this investigation. The fracture of weakly bonded composites and commercially fabricated composites will be analyzed based on considerations of the two fundamental modes. A stress criterion for noncumulative fracture will be established based on experimental data obtained from all the composite types studied. Finally, the results of a cursory study of the effects of internal filament damage on composite fracture will be presented and discussed.

Noncumulative Fracture

Radiographic evidence.- Noncumulative fracture occurred rapidly and was not preceded by individual filament breaks. There was no acoustic signal to indicate the onset of fracture, and sequential radiographs at various stages of the fracture process were extremely difficult to obtain. What is believed to be a typical sequence is represented by the pair of radiographs shown in figure 4. Both radiographs were taken through the same region of a monolayer specimen, so that identical filaments are shown in figures 4(a) and 4(b). The vertical white lines are the tungsten boride cores. The surrounding sheaths of boron are seen as dark bands adjacent to the cores, and the aluminum matrix is represented by the lighter bands separating the boron.

The radiograph of figure 4(a) reveals what appears to be the initial stage of tensile fracture in the form of several broken filaments extending inward from the edge of the specimen. The radiograph was taken through a tensile specimen which had been suddenly unloaded prior to total fracture as a result of failure of the testing machine. Apparently, noncumulative fracture had begun but was arrested by the accidental unloading. Two different filament fracture modes are observed. The third and fifth filaments from the edge of the specimen are broken cleanly, but the remaining filament breaks are characterized

by the presence of wedge-shaped fragments. The matrix between the broken filaments is still continuous and has remained visibly unaffected by the filament breaks.

In figure 4(b), the same region is shown after complete fracture of the specimen. All the additional filament breaks occurred by fragmentation, and the shape and distribution of the fragments bear a definite relationship to the direction of crack propagation. The wedge-shaped fragments are displaced in the direction of propagation, and the wedges are all oriented so that they appear as arrowheads pointing opposite to the direction of propagation.

Noncumulative fracture mechanism.- Based on the radiographs of figure 4, the following fracture mechanism is proposed: The third and fifth filaments from the edge of the specimen were weak and broke first. The elastic strain energy stored in each filament was abruptly released in the form of stress waves which propagated transversely through the matrix. The stress waves impacted against adjacent filaments with sufficient force not only to shatter them, but also to displace the fragments within the matrix. Fragments from the fourth filament were not displaced because they were in a region where two waves of approximately equal energy content were oppositely directed; therefore, their displacement was neutralized. As each successive filament was broken, the energy content of the original stress wave was alternately depleted and replenished. The wave was completely damped in figure 4(a), but above some threshold value of average filament stress, the mechanism, which will hereinafter be referred to as noncumulative filament-break propagation, became self-sustaining, and catastrophic fracture resulted.

The character of the stress wave involved in noncumulative filament-break propagation is not known. A compressive wave could produce all the observed effects, but it is difficult to imagine how a compressive wave of appreciable magnitude would be generated by fracture of a single filament. A shear wave would seem more likely to be created. In either case, it should be noted that filament fracture accompanied by fragmentation can occur without the external influence of a stress wave. The radiograph of figure 4(b) was taken after the specimen had been reloaded to failure. The filament which broke to instigate the noncumulative mechanism the second time is fragmented.

Effect of filament spacing.- The effect of filament spacing was not investigated in the sense that composite sheets with various uniform spacings were tested. That was not possible for two reasons. The first was that precise increases in the thickness of the foil used to fabricate the composite would have been necessary in order to provide the additional aluminum required to fill the increased volume between filaments. No capability existed for making such adjustments in thickness. The second reason was concerned with a limitation of the diffusion-bonding method of consolidation. It was pointed out by Dolowy (ref. 10) that the development of a strong matrix-matrix bond depended on whether the oxide films on faying foil surfaces could be ruptured before contact was made. Rupture

of the films normally occurred when the aluminum was forced into the spaces between filaments under the influence of the bonding pressure. However, when the filament spacing exceeded 1.5 diameters, rupture of the oxide films occurred only in the vicinity of the filaments where deformation was greatest. The films were left intact in the spaces between filaments, and incomplete matrix bonding was the result. It was possible, however, to fabricate B-Al sheets with small numbers of filaments missing at various locations. That was accomplished by removing filaments from monolayer preform segments before consolidation, and as many as five adjacent filaments were removed in a given location. The resulting deficiency in bond strength between matrix elements was localized, and did not seem to have a significant effect on gross specimen behavior.

A typical specimen with missing filaments is represented by the pair of radiographs presented as figure 5. Both radiographs were taken through the same region of a monolayer specimen which contained a gap created by the removal of two adjacent filaments. In figure 5(a), what may be the initial stage of noncumulative filament-break propagation is evident in the first three filaments from the specimen edge. Figure 5(b) shows the same region after complete specimen fracture. The stress wave was not damped as a result of the gap between filaments. The mechanism for noncumulative filament-break propagation described in the previous section continued across the gap to cause complete fracture of the specimen. Identical behavior was observed for specimens containing gaps produced by the removal of up to five filaments. Specimens with larger gaps were not tested; therefore, the ultimate gap width required to inhibit filament-break propagation was not determined.

Correlation with fracture surface features.- The photograph presented as figure 6 was taken of matching tensile fracture surfaces of a monolayer composite. The two halves of the specimen may be matched by mentally inserting the bulbous projection on the second filament up from the lower left corner (denoted by arrow) into its corresponding depression on the opposite surface. Two important features are observed which serve to corroborate the mechanism for noncumulative filament-break propagation discussed previously. One is the presence of wedge-shaped fragments associated with each broken filament. The second is related to fracture modes exhibited by the matrix.

Details of the matrix fracture are more visible in the magnified view of figure 7. Each broken filament lies at the bottom of an aluminum crater whose outer walls have the appearance of the shear lip in a conventional cup-cone fracture. Also, a scalloped effect is observed along the boundaries of the overall specimen fracture surface as a result of restraint imposed by the filaments on necking of the matrix. At the junctions of crater walls, the presence of gross pores resulting from microvoid coalescence indicates the fracture mode there to be ductile rupture.

All these observations indicate that matrix fracture occurred in a completely ductile manner by the normal processes of plastic flow. When the photographic evidence is combined with that obtained from analysis of the radiographs, it is apparent that isolated individual filament fractures do not initiate matrix cracks. The relatively flat transverse fracture surface is an expected result of the mechanism for noncumulative filament-break propagation, since the stress waves emanating from filament breaks impact against adjacent filaments at the point of closest approach.

Modifications of Noncumulative Fracture

The mechanism for noncumulative filament-break propagation appeared to govern the tensile strength of well-bonded composites regardless of the number of filament layers they contained. Identical evidence of the occurrence of the noncumulative mechanism was observed on fracture surfaces of composites containing as many as five layers of filament. The interpretation of radiographs became difficult, however, for trilayer and thicker materials because of overlapping filament images. For that reason, most of the subsequent discussion is restricted to fracture of monolayer or bilayer composites. Presumably, no loss of generality results from this restriction.

Initiation.- As a general rule, crack initiation occurred at a specimen edge. The radiograph presented as figure 8 shows an arrested crack extending inward from the edge of a specimen containing two layers of filament. The apparent irregularity in filament spacing is the result of looking through superimposed filament layers. The actual irregularity was not severe, as will be seen in subsequent fracture-surface observations. All the features of noncumulative filament-break propagation were present, including the displaced wedge-shaped fragments and broken filaments in advance of matrix fracture. Necking of the matrix between broken filaments could be seen in the region near the tip of the crack. Once a crack was initiated, three distinct fracture modifications were observed: transverse fracture, axial fracture, and canted fracture. Each modification was either related to or a result of noncumulative filament-break propagation. The three modifications are discussed in the following sections.

Transverse fracture.- Transverse fracture occurred when filaments from all layers in the composite failed by noncumulative filament-break propagation in a single plane perpendicular to the axis of loading. A typical transverse fracture surface of bilayer composite is shown in figure 9. The fracture morphology was very similar to that already observed for monolayer composite (figs. 6 and 7), except that in the bilayer material the crater walls intersected in a hexagonal rather than in a rectangular pattern. The magnified view of figure 10 shows details of the interior crater wall, including the shear lip and porosity at lines and points of ultimate separation in the matrix.

The shapes and arrangements of fragments associated with the fracture of filaments were typified by those shown in figures 11, 12, and 13. No attempt was made to interpret the markings on fragment surfaces. Figure 11 shows the general appearance of fragments in a single transverse fracture surface. Figure 12 does likewise but also serves to focus attention on the regions of separation between constituents of well-bonded composite. The matrix-matrix bond (denoted by arrow) has ruptured only within a very small volume in spite of the violence of a fracture process which left filament debris scattered widely. A measure of the tenacity of the filament-matrix bond was indicated by the incipient formation of dimples around the periphery of the large fragment at the bottom of the photograph. Figure 13 shows matching fragments from a single filament in two photographs taken of mating transverse fracture surfaces. Matching core segments are indicated by arrows for one fragment pair.

One unusual type of transverse fracture resulting from noncumulative filament-break propagation was not associated with the presence of wedge-shaped filament fragments. Instead of fragmenting under the influence of a transverse stress wave, the filaments broke cleanly in at least two places to form one or more relatively long cylindrical segments. Figure 14 presents radiographic evidence of that type of transverse fracture. No wedge-shaped fragments were associated with the individual broken filaments. Instead, each filament was broken cleanly in at least one additional location under the fracture surface.

A pair of matching fracture surfaces from the specimen represented in the previous radiograph (fig. 14) are shown in figure 15. Matching filaments are linked by a line. Each broken filament is split longitudinally to an unknown depth, probably down to the nearest transverse break under the surface. The splits are all parallel to the plane of the composite sheet, and thus were not obvious in the radiograph of figure 14. This is an excellent example of a situation in which failure to combine radiographic and microscopic observations would have led to confusion and possibly even an erroneous interpretation.

Most of the fracture surface examined in the present investigation was a consequence of transverse noncumulative fracture, and wedge-shaped filament fragments were abundant in the surface. Transverse fracture involving split filaments was extremely rare. In fact, it was seen only twice during observation of nearly one thousand B-Al tensile fracture surfaces. The particular area represented by figures 14 and 15 made up approximately one-third of the total fracture surface of a well-bonded monolayer specimen. The remaining two-thirds showed evidence of the more prevalent transverse fracture with wedge-shaped fragments. A study of the direction of fragment displacement indicated that crack propagation proceeded out of the region of split filaments, and that this region was the first to fracture.

Axial fracture.- The axial modification was seen as a step parallel to the axis of loading which connected two regions of transverse fracture at different levels. The radiograph of figure 16 shows the axial fracture modification in a bilayer specimen as a vertical step. Noncumulative filament-break propagation proceeded from left to right until it reached the region now identified as the step. At that point it was interrupted by the initiation and propagation of filament breaks at a different level. By studying the directions of fragment displacement, it was readily seen that secondary initiation occurred three or four filaments to the right of the step (see arrow) on the upper level. Following that, the crack continued to propagate from left to right. Fracture at the step occurred by shear rupture of the matrix parallel to the load axis.

The characteristic appearance of the axial fracture modification is seen in the matching fracture surfaces of figure 17 which show the step and evidence of noncumulative filament-break propagation on either side. The magnified view in figure 18 shows details of the axial shear surface. Note that the side of the exposed filament is covered with a residual layer of aluminum. The surfaces of this layer and the matrix both exhibit the elongated dimples which are characteristic of shear rupture in a ductile metal. The shear dimples on the exposed filament and the corresponding ones on the matching surface are shown magnified to a greater extent in figure 19.

Axial fracture occurred locally and made up only a small part of any given fracture surface. Its occurrence was always associated with the presence of a preexisting filament break located away from the edges of the specimen and apart from the region in which the filament-break propagation mechanism was operating. For some unknown reason, the previously broken filament was able to resist the stress wave impinging on its side without fragmenting in the normal manner, and thus to stop the initial transverse crack. Fragmentation sometimes occurred at a different location, and occasionally the filament split, but the preexisting break was never directly involved in the fracture of the specimen. Secondary initiation occurred immediately in the adjacent filaments, possibly because the initial crack had progressed sufficiently far into the specimen to create a significant additional increment of tensile stress due to in-plane bending. Axial separation between the two transverse fracture planes was determined by the location of the weakest point in one of the adjacent filaments which was within the region of influence of the stress concentration. Specimens which contained no preexisting filament breaks generally did not exhibit the axial fracture mode.

An example of the role of the preexisting filament break in the axial fracture modification is shown in figure 20. These are the same two radiographs presented earlier as figure 5 but cropped differently to show the vertical step. In addition to the three previously mentioned broken filaments at the edge of the specimen in the upper part of figure 20, the 27th from the edge is also broken (see arrow). This break existed before any load was applied and is shown in the lower part of figure 20 as well.

Filament-break propagation proceeded from right to left until it reached the filament with the preexisting break. That filament broke, split, and fragmented at a different location, but it succeeded in stopping the initial crack. A new series of filament breaks was then initiated on the lower level in the manner previously discussed. Occasionally when a split filament was involved, the axial fracture surface developed in such a way that the split was exhibited. Successively magnified views of a typical fracture surface of that type are shown in figures 21, 22, and 23. Figure 21 shows the general appearance of the axial fracture surface with transverse fracture at different levels on either side. Details of the overall axial surface are shown in figure 22, and a closeup view of the split filament surface is shown in figure 23. Apart from the filament split, the remainder of the axial surface was created by shear rupture as in figures 17, 18, and 19.

Canted fracture.- The third noncumulative fracture modification observed was descriptively termed canted fracture because the resulting fracture surface was angled with respect to the plane of the sheet specimen. Canted fracture occurred when filaments in adjacent layers failed by transverse break propagation in separate planes perpendicular to the load axis. Matrix failure then occurred by shear along an angled surface between filament layers.

Radiographic evidence of the canted modification of noncumulative fracture is presented in figure 24 for a bilayer specimen. In the canted region the broken ends of one filament layer extend beyond those of the other layer, and matrix thickness gradually decreases toward the extended ends. A portion of canted surface corresponding to the radiograph is presented as figure 25. The appearance bears some similarity to the chisel-point fracture observed under certain conditions in the tensile fracture of metallic sheet. Filament fracture on different transverse planes is obvious along with the canted matrix shear surface between filament layers. A magnified view of the shear surface is shown in figure 26, and exhibits the characteristic elongated dimples seen previously for the case of axial shear.

A characteristic feature of canted fracture surfaces observed in this study is a narrow strip on exposed filament sides where no bond existed between filament and matrix. Evidence of the unbonded strip is obvious for three filaments in figure 25, particularly the one with the greatest amount of its side exposed. The unbonded strip on the side of that filament is shown in greater detail in figure 27(a). The opposing filament fracture surface is shown in figure 27(b). Note the absence of shear dimples on the matrix surface where the unbonded strip pulled out. The presence of the unbonded areas is probably due to incomplete removal of the acrylic resin binder used during fabrication to maintain filament spacing and alinement. The influence, if any exists, of these unbonded areas on the occurrence of canted fracture is not known.

Canted fracture is a local phenomenon which is almost always found to comprise a very small portion of multilayer composite fracture surfaces. The fracture surface of figure 25 is typical in that it contains at least one filament which is apparently unfragmented. The fact that occasionally filaments are found which exhibit whole fracture surfaces, even in a generally noncumulative fracture, indicates that failure of these filaments possibly occurs as a result of simple axial tension rather than under the influence of a transverse impact.

Fracture of filaments.- Very little is known of the mechanisms by which individual boron filaments fracture. The experimental observation that some filament fractures are accompanied by fragmentation while others fail without fragmenting may be a result of different states of stress acting on the filaments. Fracture associated with fragmentation might be expected to occur when a localized bending stress is applied to a filament already in axial tension, and would probably initiate at a surface flaw in the region of highest tensile stress. In the absence of bending, fracture without fragmentation might be more likely and could be initiated in the core of the filament. A typical pair of matching whole-filament fracture surfaces are presented in figure 28. The crack has proceeded through the boron sheath with a turning and climbing motion to produce a fracture surface in the form of a spiral ramp. The point of initiation is not known.

A second consideration is that boron filaments may naturally exhibit two different fracture modes, depending on the history of manufacturing and processing. It was observed in a previous investigation (ref. 9) as well as in the present study that filaments with extremely low strengths did not generally fragment when they were individually loaded to failure in tension. In some cases, the low strengths were a characteristic of poor-quality filament, and in other cases they resulted when good-quality filament was subjected to various combinations of heat and pressure prior to testing under ambient conditions.

Cumulative Fracture

By using consolidation pressures greater than 69 MN/m^2 (10 ksi), it was possible to fabricate batches of well-bonded composite with varying degrees of filament degradation. When filaments in a given batch had been degraded beyond a certain level, composite specimens from that batch no longer fractured in a completely noncumulative manner. Sporadic acoustic emissions prior to total specimen failure indicated that filaments were breaking, both individually and in groups, and that the composite fracture mode had become at least partially cumulative. Since cumulative fracture occurred much more slowly than noncumulative fracture, it was a comparatively simple task to arrest a cumulative crack for further study.

Radiographic evidence.- A typical cumulative crack in well-bonded bilayer composite is shown in the radiograph of figure 29, growing inward from the edge of a specimen. Most of the filaments broke without fragmenting, and when fragmentation did occur, the displacement of fragments was randomly directed. One similarity between noncumulative and cumulative fracture was that individual filament breaks did not produce matrix cracks. In both modes, broken filaments were observed several interfilament spacings in advance of ductile separation of the matrix. A major difference between the noncumulative and cumulative modes was observed in the paths along which cracks propagated. In contrast with the relatively straight transverse crack associated with noncumulative fracture, the cumulative crack changed direction frequently as it passed through the specimen.

The cumulative fracture mechanism.- The crack shown in figure 30 is an excellent example of cumulative filament-break propagation as described by Zweben in references 2 and 11. Fracture begins when one or two filaments break near the edge of a specimen, probably under the influence of a stress concentration produced by machining. The presence of broken filaments contributes an additional increment of stress concentration, or as Zweben explains, a load concentration which is effective over a finite length of the adjacent filaments rather than at a point. The strength of boron filaments varies from filament to filament and from point to point along the length of a single filament. Thus there are two nonexclusive possibilities for subsequent filament fracture, both of which are observed near the crack tip in figure 29: The load concentration acting over a length of a given filament resulting from the breaking of a neighbor can cause the filament to break at a weak point located some distance above or below the break in the neighboring filament. Also, a weak point can be located so that several filaments immediately adjacent to a broken filament will remain whole while another filament breaks farther away. The load concentration is less on the more remote filament, but still effective. The tortuous path of the crack is explained by this reasoning. The crack proceeds gradually from one group of broken filaments to the next even though the axial separation between the groups may be large. If adjacent breaks or groups of breaks are widely separated in the direction parallel to the axis of loading, then matrix fracture occurs by axial shear. There is a great deal more axial shear in cumulative fracture than in the noncumulative mode.

The observation that filaments fracture several interfilament spacings in advance of matrix fracture probably holds true for any composite with a ductile metal matrix. The same behavior was observed by Cooper and Kelly (ref. 12) for tungsten-wire-reinforced copper composites.

A small number of filament breaks were characterized by the presence of wedge-shaped fragments, which indicates that fracture of those filaments was influenced by

transverse stress pulses emanating from neighboring filament failures. In the specimen of figure 29, fragmented breaks were widely dispersed, and the direction of fragment displacement depended solely on the direction from which the stress wave came. The local stress in the regions where fragmentation occurred never reached the level required to sustain the mechanism for noncumulative filament-break propagation.

The radiograph of figure 29 shows completely cumulative fracture. When fracture occurred by a combination of the cumulative and noncumulative modes, a cumulative region was developed sometimes at an edge of a specimen and sometimes within its interior. That region grew in size until the stress in the composite became sufficient to cause instantaneous fracture of the remainder of the specimen by noncumulative filament-break propagation. The radiograph of figure 30 shows a bilayer specimen after complete mixed-mode fracture. Only the cumulative region is shown, and it was bounded on both sides by noncumulative fracture of the transverse type. This radiograph will be used in the following discussion of the features of cumulative fracture surfaces.

Cumulative fracture surfaces.- The two matching fracture surfaces corresponding to the radiograph in figure 30 are presented as figures 31 and 32. The same surfaces are shown in both figures, but they have been rotated so that the surface hidden in one figure can be seen in the other. The fracture surfaces of figure 31 may be related to the radiograph of figure 30 by the segment of broken filament which protrudes horizontally from the near surface. The radiograph shows two such segments; apparently one was lost before the fracture surface was photographed. The fracture surface of figure 32 may be related to the radiograph by the same filament segment, and also by a small piece of composite which is cantilevered from the surface at one end of the cumulative region.

Figures 31 and 32 show the irregularity and angularity of typical cumulative fracture surfaces. The filaments in the cumulative region are mostly unfragmented, and to a large extent, matrix fracture is the result of axial or nearly axial shear. On either side of the cumulative region, the fracture surfaces become transverse, and the proportion of fragmented filaments increases rapidly; these features indicate the onset of the noncumulative mode of fracture.

Canted fracture.- Canted fracture was previously described as a modification of noncumulative fracture. However, in the upper left corner of figure 31, a region of canted fracture separates the cumulative and transverse noncumulative regions. This canted surface is isolated in figure 33, and like all other canted fracture surfaces, it contained at least one unfragmented filament. Canted fracture probably occurred as the transition between the noncumulative and cumulative modes. In fractures which were previously referred to as being completely noncumulative, the presence of a few small regions of canted fracture probably represented incipient cumulative fracture which failed to develop further because of the rapidity of the noncumulative fracture mechanism.

Fracture of Weakly Bonded Composite

One batch of B-Al composite sheet was fabricated so that internal bonding between constituents was relatively weak. It was impossible to distinguish between fractures of well-bonded and weakly bonded material from observations of radiographs. The fracture surfaces, however, reflected the difference in bond strengths. A pair of matching fracture surfaces from a typical weakly bonded specimen are shown in figure 34. Tensile fracture was only partially cumulative; therefore, most of the broken filaments were fragmented. Evidence of weak bonding was obvious, both in the separation of foil layers upon ductile failure of the matrix (see arrows) and in local filament-matrix debonding in the immediate vicinity of broken filaments. Debonding between filaments and matrix is more obvious in the magnified view of figure 35 in the form of annular chasms separating the filaments from the surrounding matrix.

In the work of Mullin et al. on fracture of boron-epoxy composites (refs. 6 and 7), matrix cracking was a primary feature of the noncumulative mode of fracture. They found that a slight amount of filament-matrix debonding in the vicinity of a broken filament could absorb a significant quantity of the elastic strain energy released by the filament to prevent cracking of the matrix. They could thus postpone the onset of noncumulative fracture by weakening the filament-matrix bond. The noncumulative fracture mode in B-Al composite sheet resulted from the transverse propagation of a stress wave emanating from an individual filament fracture. That stress wave was not damped by weak bonding, and since it had already passed through the area, its effect was not diminished by subsequent local debonding due to shear stress concentrations at newly formed filament ends.

Fracture of Commercially Fabricated Composite

Two different commercially fabricated B-Al composites were included in the present investigation. One material contained five layers of 0.10-mm-diameter (0.0041-in.) silicon-carbide-coated boron filament in a 2024 aluminum alloy matrix. Consolidation had been accomplished by diffusion bonding in such a way that the material could be classified as weakly bonded. The second commerically fabricated composite contained only one layer of 0.14-mm-diameter (0.0056-in.) boron filament in a 6061 aluminum alloy matrix. It was also consolidated by diffusion bonding, but in such a way that varying bond strength was produced within the material.

A typical fracture surface for the five-layer commercial material is presented as figure 36, and gives an indication of the complexity of the fracture process for multilayer composites in general. Beginning at the left edge of the specimen, the fracture mode was transverse noncumulative. A short distance to the right, the mode became cumulative. The cumulative region blended into a second transverse noncumulative region, and so on.

All the modes and modifications of fracture discussed previously were present in the fracture surface. In addition, there was evidence of debonding between matrix layers and between filaments and matrix resulting in filament pull-out.

Several of the more important features of the fracture surface of figure 36 are presented for more detailed examination in the sequence of figures 37, 38, and 39. Figure 37 shows the leftmost transition between the transverse noncumulative and cumulative modes. Transverse, axial, and canted fracture can all be identified in the photograph, along with evidence of poor filament-matrix bonding. Figure 38 shows the second region of transverse noncumulative fracture and evidence of weak matrix-matrix bonding in the form of troughs which developed as individual matrix layers separated in an attempt to neck down independently. Figure 39 shows local debonding between filaments and matrix at the left edge of the second transverse noncumulative region. The rough, cluttered appearance of the matrix fracture surface is typical of a ductile fracture surface for aluminum alloys (2024 in this case), and serves to justify the choice of relatively pure aluminum (the 1230 alloy) for the majority of specimens observed in the research program.

The monolayer commercial material was obtained in the form of a 61- by 15-cm (24- by 6-in.) sheet. The sheet was not uniformly consolidated, and tensile specimens cut from the sheet were moderately weakly bonded or extremely weakly bonded, depending on their locations in the sheet. The moderately weakly bonded specimens failed by noncumulative filament-break propagation. A typical transverse fracture surface is shown in figure 40 and an axial surface, in figure 41. Evidence of moderately weak bonding is seen in the transverse surface as separations in the matrix between filaments where individual foils attempted to neck down independently. In the axial surface, the side of the exposed filament is bare, indicating a weak filament-matrix bond.

Specimens for which internal bonding was extremely weak failed cumulatively. A portion of a typical fracture surface is presented as figure 42. Evidence of extremely weak bonding is seen in the regions between filaments where the matrix-matrix bond was never formed, and in extensive pull-out of filaments. Several specimens were so weakly bonded that both aluminum foils separated from the filaments prior to failure of the specimen. This behavior was exhibited by the tensile specimen shown in figure 43. The delamination occurred while the specimen was being loaded, and the filaments continued to bear load. Some of the filaments visible in figure 43 have not yet failed.

Stress Criterion for Noncumulative Fracture

Based on radiographic analyses of tensile fracture in unidirectional B-Al composite sheet, a mechanism of noncumulative fracture has been identified which severely limits the ultimate strength of the material. The mechanism has proven to be consistent with commonly observed features of composite tensile fracture surfaces. It was observed

during the course of the investigation that variation of the pressure used to consolidate well-bonded composite caused the fracture mode to change, and it was assumed that the change resulted from a varying degree of filament degradation, even though the nature of the degradation resulting solely from a pressure change was not known. By comparing the average filament stress at the instant of composite fracture with the distributed strengths of filaments contained within that composite, the filament stress level required to initiate and sustain noncumulative fracture was determined. That comparison was made for six batches of well-bonded composite with fracture modes varying from completely noncumulative to completely cumulative in order to establish a threshold value of average filament stress below which the noncumulative mechanism was not operative. The comparison was also made for the two commercially fabricated composites and the weakly bonded composite in an attempt to determine whether the results of the comparison for well-bonded composites were generally applicable.

Comparison of average filament stress at composite fracture with strengths of filaments in a composite.- This comparison was made for six batches of well-bonded composite sheet, each with a different degree of filament degradation. Two batches exhibited completely noncumulative fracture; three batches failed by a combination of the noncumulative and cumulative modes; and one batch failed in a completely cumulative manner. The comparison was also made for the two commercially fabricated composites and one batch of weakly bonded composite.

The first comparison is shown in figure 44 for a monolayer composite containing 0.14-mm-diameter (0.0056-in.) boron filament. The composite was consolidated by hot-pressing under a pressure of 69 MN/m^2 (10 ksi). Filament strength was characterized by the failure-frequency histogram shown. The histogram was constructed by plotting the percentage of filament failures observed within stress intervals of 69 MN/m^2 (10 ksi); the failures were based on tensile tests of 150 filament specimens chemically removed from three typical composite tensile specimens. The weakest filament encountered exhibited a strength of approximately 1.72 GN/m^2 (250 ksi). Fifteen additional composite tensile specimens were prepared from the same batch, and tested to determine the average filament stress at fracture of the composite. That was done by assuming that the average filament strain was identical with the measured composite strain at failure of a specimen. Average filament stress was calculated by multiplying the measured ultimate strain value by Young's modulus of the boron filament, 380 GN/m^2 (55×10^3 ksi). The results are shown as the vertical scatter band at the left side of the histogram. The average filament stress at composite fracture (represented by the vertical dashed line within the scatter band) was identical with the strength of the weakest filament in the composite.

The comparison given in figure 44 is representative of well-bonded composite in which the filaments are not too severely degraded. The strength distribution for virgin 0.14-mm-diameter (0.0056-in.) filament is presented as figure 45 to provide an indication of the actual degradation involved. For composite of this quality, enough energy is released by fracture of the weakest filament to initiate and sustain catastrophic filament-break propagation. Thus, fracture is completely noncumulative. Strength data from tests of virgin 0.14-mm-diameter (0.0056-in.) filament are listed in table I. Strength data for the reclaimed filaments are given in table II and the filament stress from the composite tensile tests is presented in table III, identified as batch 44.

Similar comparisons were made for five additional batches of bilayer composite containing 0.099-mm-diameter (0.0039-in.) boron filament. The virgin-strength distribution for this diameter filament is presented in figure 46, which is plotted from data listed in table IV. The additional bilayer composites were still well bonded, but filament degradation had been intentionally made more severe in each successive batch. The second comparison is made in figure 47(a) for a bilayer composite which contained slightly weaker filaments. The average filament in the composite had a strength of 2.07 GN/m^2 (300 ksi) compared with 2.48 GN/m^2 (360 ksi) for the previous batch represented by figure 44. Both composites were consolidated under a pressure of 69 MN/m^2 (10 ksi), but the smaller initial filament diameter in the bilayer composite apparently made the degradation more effective in reducing the ability of the filament to withstand load. The weakest filament had a strength of 1.31 GN/m^2 (190 ksi), and again, that value was identical with the average filament stress at failure of the composite. Fracture was still completely noncumulative. The histogram of figure 47(a) represents the results of 100 tensile tests of reclaimed filaments. The data are listed in table V, identified as batch 47. Twenty composite specimens were tested from the same batch to determine the average filament stress at composite failure. Those data are listed in table III.

In figure 47(b), data are plotted for a composite which had been consolidated under a pressure of 76 MN/m^2 (11 ksi). The average filament strength was reduced to 1.90 GN/m^2 (275 ksi), and the average filament stress at fracture of the composite was 1.18 GN/m^2 (171 ksi). For the first time there were filaments in the composite which had strengths less than the average filament stress at fracture of the composite, and those filaments failed cumulatively before the noncumulative mode was initiated. The data for figure 47(b) are listed in tables VI and III, identified as batch 48.

The data in figure 47(c) are from a composite in which the filaments were degraded to an even greater extent, exhibiting an average strength of 1.76 GN/m^2 (255 ksi). The average filament stress at composite failure, however, did not decrease, but remained essentially constant at 1.19 GN/m^2 (173 ksi). This material was hot pressed under a

pressure of 83 MN/m^2 (12 ksi) and was designated as batch 49. Data from filament and composite tests are presented in tables VII and III, respectively, for this batch.

The comparison made in figure 47(d) is for composite which had been consolidated under a pressure of 90 MN/m^2 (13 ksi). The average strength of filaments leached from the composite was only 1.55 GN/m^2 (225 ksi). The average filament stress at fracture of the composite, however, still remained constant at a value of 1.19 GN/m^2 (173 ksi). The filament and composite tensile data for this composite are listed in tables VIII and III, respectively, identified as batch 50.

The final comparison for well-bonded composite is made in figure 47(e) for material which had been consolidated by hot-pressing under a pressure of 103 MN/m^2 (15 ksi). Of all the composites tested, this material contained the most severely degraded filaments. Fracture of the composite was completely cumulative. The average filament in the composite had a strength of 1.62 GN/m^2 (235 ksi), which was slightly greater than the value of 1.55 GN/m^2 (225 ksi) for the previous case of batch 50, but the increased degradation was seen as a broadening of the range over which the filament strengths were distributed. The average filament stress at composite fracture was 1.05 GN/m^2 (152 ksi), which is significantly less than the value of approximately 1.17 GN/m^2 (170 ksi) observed for composites which failed in a partially cumulative mode. Data from filament and composite tensile tests are listed in tables IX and III, respectively, identified as batch 51.

A similar comparison was made for the weakly bonded composite which was consolidated at 783 K (950° F) under 62 MN/m^2 (9 ksi) pressure. Results for the weakly bonded composite are presented in figure 48, plotted from the data in tables X and III. The average filament strength in the composite was 1.86 GN/m^2 (270 ksi), and the average filament stress at fracture of the composite was 1.22 GN/m^2 (177 ksi). The average filament stress resulting from composite tensile tests was in reasonably good agreement with the previous results from composites which underwent partially cumulative fracture. However, the average filament strength was somewhat lower than had been expected considering the relatively mild hot-pressing conditions. It should be recalled that the weakly bonded composite contained 0.089-mm-diameter (0.0035-in.) boron filament which exhibited highly variable strength based on qualitative observations during filament winding. However, the virgin-strength distribution was not qualitatively determined, and as a result, the true extent of degradation resulting from consolidation could not be evaluated.

Results from tests of the commercially fabricated five-layer composite are presented in figure 49. The data from these tests are listed in tables XI and III. The material contained 0.10-mm-diameter (0.0041-in.) silicon-carbide-coated boron filament in a 2024 aluminum alloy matrix. The average filament strength was reasonably high at 2.14 GN/m^2 (310 ksi), but the distribution was dispersed over a 3.17 GN/m^2 (460 ksi)

range. The average filament stress at composite fracture was 1.14 GN/m^2 (165 ksi), not greatly different from the previously observed value for composites which failed in a partially cumulative manner.

The commercially fabricated monolayer composite contained 0.14-mm-diameter (0.0056-in.) boron filament in a 6061 aluminum alloy matrix, and exhibited different fracture characteristics depending on whether it was moderately weakly bonded or extremely weakly bonded. The moderately weakly bonded composite behaved in a manner similar to the composites which were fabricated at the Langley Research Center except that filament degradation was minimal. The average filament stress at composite fracture and the strength of filaments in the composite are compared in figure 50 for moderately weakly bonded specimens. The high average filament strength, 3.79 GN/m^2 (550 ksi), indicated that almost no degradation of filaments resulted from consolidation of the composite. The average filament stress at composite fracture, 2.65 GN/m^2 (384 ksi), was once again approximately equal to the strength of the weakest filament in the composite. The data from tests of filaments and composite specimens are listed in tables XII and III, respectively, for the moderately weakly bonded material.

In every tensile test of an extremely weakly bonded specimen of the commercially fabricated monolayer composite, some delamination occurred prior to total fracture. As a result, it was impossible to obtain a meaningful value of ultimate strain. For that reason, a comparison of average filament stress at composite fracture with the strength of filaments in the composite was not made for extremely weakly bonded specimens.

The commercially fabricated monolayer material is representative of the best quality B-Al composite currently available. On the average, fracture of the material was precipitated by failure of the weakest filament, but fabrication parameters had been adjusted so that filament degradation was minimized, and the weakest filament still had considerable strength. This material contained 35 percent filaments by volume and exhibited a composite tensile strength in excess of 1.0 GN/m^2 (150 ksi). Even in regions where internal bonding was extremely weak, composite tensile strengths of 0.8 GN/m^2 (120 ksi) were realized.

Threshold stress for noncumulative fracture.- At this point it has been demonstrated that the tensile fracture mode for unidirectional B-Al composite sheet can be altered at will from completely noncumulative to completely cumulative through a range of mixed-mode fracture. It will now be shown that a threshold value of average filament stress exists above which composite fracture is completely noncumulative, and below which fracture occurs in a completely cumulative manner. In order to show this, it is necessary to represent collectively the essential information presented in figures 44 and 47 to 50 in a single graph. This is accomplished in figure 51, where average filament stress at com-

posite fracture is related to the strength distributions of filaments leached from the several composite batches.

In figure 51, the average filament stress at composite fracture is plotted as a function of a degradation factor, which is defined as that fraction of distributed filament strengths which were greater than or equal to the average filament stress at composite fracture. For completely noncumulative fracture, the degradation factor is unity. The data from figure 44, for example, are represented by the next to uppermost point in figure 51, and the degradation factor is unity since all the filaments tested had strengths greater than the average filament stress when composite fracture occurred.

The data of figure 51 seem to indicate, for all the composites represented, that unidirectional B-Al composite sheet will fail in tension as the result of noncumulative filament-break propagation initiated by failure of its weakest filament, provided the average filament stress remains above approximately 1.17 GN/m^2 (170 ksi). That was the behavior observed for the composites represented by the upper three data points (composites of figs. 44, 47(a), and (50)). Since completely noncumulative fracture is apparently triggered by failure of the weakest filament in the composite, it would be essential to know what the strength of that filament is. A knowledge of the average filament strength would be of little value in predicting composite strength.

The lower data point in figure 51 represents the well-bonded composite of figure 47(e) in which filaments were most severely degraded, and for which fracture was completely cumulative. Isolated filaments in this composite were fragmented, but the average filament stress never reached the critical value required to sustain the noncumulative fracture mechanism.

The composites of figures 47(b), 47(c), 47(d), 48, and 49 contained appreciable numbers of weaker filaments, but did not fracture until the average filament stress reached approximately 1.17 GN/m^2 (170 ksi). Those composites are represented in figure 51 by the five data points associated with the horizontal line at 1.17 GN/m^2 (170 ksi). All five composites underwent fracture by a combination of the cumulative and noncumulative modes. The weaker filaments failed cumulatively until the average stress in the remaining filaments reached the limiting value of 1.17 GN/m^2 (170 ksi). At that stress, the mechanism for noncumulative filament-break propagation was initiated, became self-sustaining, and resulted in abrupt failure of the remaining filaments and the composite. For composites which underwent mixed-mode fracture, the degradation factor could be defined as the fraction of filaments which were directly involved in the noncumulative mode of fracture.

The limiting value of 1.17 GN/m^2 (170 ksi) appears to be the threshold stress for the initiation and sustenance of the mechanism for noncumulative filament-break propagation in B-Al composite. On the average, any single filament which fractures at a tensile

stress greater than 1.17 GN/m^2 (170 ksi) will liberate sufficient elastic strain energy to initiate a self-sustaining progression of filament fractures similar to a chain reaction. Immediate composite fracture is the result. The strain energy from a filament which fractures at a stress less than 1.17 GN/m^2 (170 ksi) will be absorbed without causing the immediate fracture of a sufficient number of adjacent filaments to initiate the noncumulative mechanism.

It is important to note that figure 51 presents results from composites containing one, two, and five filament layers. The composites contained boron filaments with diameters of 0.089 mm (0.0035 in.), 0.099 mm (0.0039 in.), and 0.14 mm (0.0056 in.) as well as 0.10-mm-diameter (0.0041-in.) silicon-carbide-coated boron filament. Both well-bonded and moderately weakly bonded composites containing three markedly different matrix alloys are represented. None of these differences seem to affect the general applicability of the fracture mechanism for noncumulative filament-break propagation or the minimum stress required for its initiation.

Fracture of Internally Damaged Composites

Fifteen composite tensile specimens were prepared with internal filament damage. An attempt was made to cut a number of adjacent filaments transversely in the center of the gage section of each specimen prior to consolidation. Actually, instead of being cut, the affected filaments were crushed, and the internal damage after consolidation was much less localized than had been planned. The number of damaged filaments per specimen ranged from four to 20 out of a total of 100 in a typical specimen. A radiograph taken through the flawed region in a specimen containing four damaged filaments is presented as figure 52. The matrix was continuous around the broken filaments, and the adjacent whole filaments showed some tendency to be washed into the flawed region by matrix flow during diffusion bonding. The flawed region of a specimen containing 14 damaged filaments is shown in the radiograph of figure 53, against a background formed by a strain-gage grid.

All 15 flawed specimens failed in their gage sections, but not one failure was associated with an internal flaw. Whatever stress concentrations there were associated with the internal filament breaks were made negligible by plastic flow in the matrix in the immediate vicinity of the breaks. Further, the broken filaments were rendered ineffective in carrying load only in the flawed region and over the short distance required to reassume the load by shear transfer through the matrix. So long as the matrix in a flawed region remained continuous, a relatively large number of broken filaments (up to 20 percent of the total number in the specimen in the present investigation) could be present in the region without influencing fracture of the specimen.

CONCLUDING REMARKS

The results of this investigation have shown that the tensile strength of composite sheet of aluminum unidirectionally reinforced with boron filament (B-Al) was generally limited by a noncumulative fracture mechanism which involved the initiation and sustenance of a chain reaction of filament fractures at a relatively low stress level. Matrix fracture followed in a completely ductile manner. The mechanism was apparently initiated by the first few filaments to break above a threshold stress level of approximately 1.17 GN/m^2 (170 ksi), and was perpetuated by the transverse propagation of stress waves within the composite which caused rapid fracture of the remaining filaments. Within the limited ranges investigated, the threshold stress for initiation of the noncumulative mechanism was not altered by variations in filament diameter, number of filament layers, strength of interfacial bonds, or the identity of the aluminum alloy matrix.

A comprehensive analysis of tensile fracture surfaces revealed that characteristic features of the surfaces were determined by the mode of fracture: cumulative, partially cumulative, or noncumulative. The characteristic features were categorized and related to the responsible fracture mechanisms in such a way that subsequent fractographic analyses of B-Al tensile failures should be facilitated by direct comparison with the results of this investigation.

Tests of specimens which contained flaws in the form of internally broken filaments revealed that a relatively large proportion (up to 20 percent in this investigation) of the filaments in a given specimen may be broken without directly affecting fracture. Local stress concentrations resulting from internal filament breaks were apparently alleviated by matrix plasticity.

Future research designed to improve the strength of B-Al composite should be concerned with the problem of internally damping the stress wave produced by the failure of individual filaments. Also, it would seem wise to consider means for narrowing the range over which the strengths of boron filaments are spread. Even the strength of good-quality, well-bonded composite with minimal filament degradation is apparently limited by the strengths of its weakest few filaments.

Langley Research Center,
National Aeronautics and Space Administration,
Hampton, Va., March 9, 1972.

APPENDIX A

CONVERSION OF U.S. CUSTOMARY UNITS TO SI UNITS

The International System of Units (SI) was adopted by the Eleventh General Conference on Weights and Measures, Paris, October 1960 (ref. 8). Conversion factors for the units used herein are given in the following table:

Physical quantity	U.S. Customary Unit	Conversion factor (*)	SI Unit (**)
Length	in.	2.54×10^{-2}	meters (m)
	ft	3.048×10^{-1}	
Stress	ksi	6.895×10^{6}	newtons per square meter (N/m^2)
Temperature	($^{o}F + 459.67$)	5/9	Kelvins (K)

*Multiply value given in U.S. Customary Unit by conversion factor to obtain equivalent value in SI Unit.

**Prefixes to indicate multiple of units are as follows:

Prefix	Multiple
milli (m)	10^{-3}
centi (c)	10^{-2}
kilo (k)	10^{3}
mega (M)	10^{6}
giga (G)	10^{9}

APPENDIX B

COMPOSITE FABRICATION

Filament-Winding Apparatus

A combined filament-winding and diffusion-bonding process was used to produce the B-Al composite in the form of unidirectionally reinforced sheet. The apparatus constructed for filament winding is shown in figure 54. Boron monofilament was taken off the manufacturer's reel, passed across a traversing mechanism, and wound onto a cylindrical mandrel covered with a single layer of aluminum foil. The mandrel was driven by a variable-speed electric motor through a reduction gear. The traversing mechanism used to locate the filament on the mandrel surface was gear driven at a constant speed. Smooth filament tension was provided by magnetically braking the payoff reel. The shaft of the reel was coupled to the shaft of a three-phase induction motor whose stator winding was connected to provide maximum magnetic coupling with its rotor when dc current was passed through the motor. Continuously variable braking action was obtained by passing the ac output from a variable transformer through a full-wave silicon rectifier into the motor.

Filament spacing was controlled by varying the speed of mandrel rotation, but the existing speed-control device was not sufficiently stable in the presence of minor line-voltage fluctuations to permit accurate filament placement. To eliminate that problem, a stroboscopic tachometer was set at the desired speed for the mandrel drive motor. Precise speed control was achieved by continuous manipulation of a 10-turn potentiometer added to the existing speed control to match the speed of the stroboscopic flash. Once a satisfactory winding apparatus had been developed, it was possible to make an advance calculation of the desired filament spacing, and then to duplicate the calculated value in practice with an error of less than 0.4 percent per cm of traverse (1.0 percent per in.).

Fabrication of Monolayer Preform

A 10.2-cm-wide (4.0-in.) sheet of 0.076-mm-thick (0.003-in.) 1230 aluminum alloy foil was wrapped around the circumference of a 24.1-cm-diameter (9.5-in.) wooden mandrel so that the ends butted precisely together. The 1230 aluminum alloy was chosen because it was available in copious quantities at the Langley Research Center and because its purity (99.3 percent Al) would insure the production of clean, precipitate-free fracture surfaces. The exposed surface of the foil was transversely brush painted with an air-drying acrylic resin solution (Rohm and Haas "Acryloid B-66") which dried with sufficient tack to maintain filament spacing and alinement. The resin formulation was one of several available which would evaporate completely during subsequent consolidation of the

composite. Either 0.099-mm-diameter (0.0039-in.) or 0.14-mm-diameter (0.0056-in.) boron filament was wound at 79 or 63 per cm (200 or 160 per inch), respectively, onto the resin-coated surface of the foil, and a second coating of resin was applied to the layer of filaments. Once the resin was dry, foil and filaments were removed from the mandrel as a 76-cm-long (30-in.) unit by cutting through the filaments along the butt between foil ends. The resin binder was sufficiently pliable when dry to allow relative longitudinal motion of constituents when the monolayer foil-filament preform was flattened, yet there was no lateral displacement of filaments. The flat preform was cut into rectangular segments 7.6 cm (3.0 in.) wide by 17.8 cm (7.0 in.) long with their length parallel to the filament direction. The segments were stacked in the sequence Al-B/Al-B/. . ./Al as desired in preparation for consolidation by diffusion bonding.

Diffusion Bonding

Consolidation of filaments and foil into composite sheet was accomplished by diffusion bonding the stacked preform segments in an evacuated stainless steel retort. A thin, water-base slurry of powdered magnesium oxide was applied as a parting agent between the retort and the composite. Retort pressure was maintained below 0.133 N/m^2 (10^{-3} mm Hg). The retort and its contents were heated from ambient temperature to 700 K (800° F) under contact pressure between electrically heated platens installed in a hydraulic testing machine with a capacity of 1.33 MN (300 kip). The temperature was held for 15 minutes to allow the resin binder to evaporate. Pressure was then applied through the platens as they were heated to the bonding temperature.

In most cases, bonding temperature was 866 K (1100° F) and bonding pressure was 69 MN/m^2 (10 ksi). These severe conditions were used to insure well-bonded composite. Sheet material with reproducible properties was required, and to that end, the decline in average composite strength resulting from increased filament degradation was accepted. In several instances, bonding pressures as high as 103 MN/m^2 (15 ksi) were used to influence the degree of filament degradation resulting from consolidation. Both the temperature and the heating rate were electronically controlled during the heating portion of the diffusion-bonding cycle. The rate of temperature increase was 16.7 K/min (30° F/min), and the instantaneous temperature varied no more than ±1.7 K (±3° F) from its intended value. The bonding temperature was maintained for 1 hour. The bonding pressure, however, was not relaxed until the retort had cooled to 422 K (300° F) in order to prevent buckling of individual filaments under the compressive stress generated by the different thermal-contraction tendencies of aluminum and boron. The cooling portion of the cycle was not controlled, but the time required for cooling to 422 K (300° F) was approximately 2.5 hours.

In one case, both pressure and temperature were reduced to 62 MN/m^2 (9 ksi) and 783 K (950° F) in order to produce composite sheet in which filament-matrix and matrix-matrix bond strengths would be weakened, and approximate those usually found in commercially fabricated composites. The weakly bonded composite was inadvertently made with substandard filament. A reel of boron filament normally contains approximately 10.7 km (35 000 ft) of filament made up of spliced lengths not less than 0.3 km (1000 ft). These smaller lengths are produced consecutively in the same run, and result from breaks which occasionally occur during production. In one reel used to fabricate specimens for this study, the manufacturer had spliced in several lengths of a 0.089-mm-diameter (0.0035-in.) filament at random. This filament was unusually weak as evidenced by the abnormally high frequency of breaks during filament winding. All except one length were detected and discarded as they came off the reel. The remaining length found its way into the weakly bonded composite.

Sheets of B-Al composite containing from one to five layers of filaments were fabricated. The filament volume fraction varied from 0.20 for a monolayer composite to 0.45 for a five-layer composite, both containing 0.099-mm-diameter (0.0039-in.) filament. The 0.14-mm-diameter (0.0056-in.) filament was only used to fabricate monolayer sheet, and the volume fraction of filaments was 0.33.

REFERENCES

1. Herring, Harvey W.; Carri, Robert L.; and Webster, Rosa C.: Compressive Behavior of Titanium Alloy Skin-Stiffener Specimens Selectively Reinforced With Boron-Aluminum Composite. NASA TN D-6548, 1971.
2. Zweben, Carl: Tensile Failure Analysis of Fiber Composites. AIAA J., vol. 6, no. 12, Dec. 1968, pp. 2325-2331.
3. Zweben, Carl: Tensile Strength of Fiber-Reinforced Composites: Basic Concepts and Recent Developments. Composite Materials: Testing and Design, Spec. Tech. Publ. STP 460, Amer. Soc. Testing Mater., 1969, pp. 528-539.
4. Zweben, C.; and Rosen, B. W.: A Statistical Theory of Material Strength With Application to Composite Materials. J. Mech. Phys. Solids, vol. 18, no. 3, June 1970, pp. 189-206.
5. Rosen, B. Walter: Mechanics of Composite Strengthening. Fiber Composite Materials, Amer. Soc. Metals, c.1965, pp. 37-75.
6. Mullin, J.; Berry, J. M.; and Gatti, A.: Some Fundamental Fracture Mechanisms Applicable to Advanced Filament Reinforced Composites. J. Compos. Mater., vol. 2, no. 1, Jan. 1968, pp. 82-103.
7. Gatti, A.; Mullin, J. V.; and Berry, J. M.: The Role of Bond Strength in the Fracture of Advanced Filament Reinforced Composites. Composite Materials: Testing and Design, Spec. Tech. Publ. STP 460, Amer. Soc. Testing Mater., 1969, pp. 573-582.
8. Comm. on Metric Pract.: ASTM Metric Practice Guide. NBS Handbook 102, U.S. Dep. Com., Mar. 10, 1967.
9. Herring, Harvey W.: Selected Mechanical and Physical Properties of Boron Filaments. NASA TN D-3202, 1966.
10. Dolowy, J. F., Jr.: Fabrication and Processing Mechanisms Active in Aluminum-Boron Composites. Metal-Matrix Composites, DMIC Mem. 243, Battelle Mem. Inst., May 1969, pp. 7-9. (Available from DDC as AD 695 046.)
11. Zweben, C.: On the Strength of Notched Composites. J. Mech. Phys. Solids, vol. 19, no. 3, June 1971, pp. 103-116.
12. Cooper, G. A.; and Kelly, A.: Tensile Properties of Fibre-Reinforced Metals: Fracture Mechanics. J. Mech. Phys. Solids, vol. 15, no. 4, July 1967, pp. 279-297.

TABLE I. - STRENGTHS OF VIRGIN BORON FILAMENTS

0.14 mm (0.0056 in.) IN DIAMETER

Strength, GN/m^2	(ksi)	Strength, GN/m^2	(ksi)	Strength, GN/m^2	(ksi)	Strength, GN/m^2	(ksi)
2.36	(342)	3.38	(490)	3.68	(534)	3.84	(557)
2.37	(344)	3.39	(492)	3.69	(535)	3.85	(559)
2.46	(357)	3.40	(493)	3.72	(539)	3.86	(560)
2.48	(359)	3.41	(494)	3.73	(541)	3.86	(560)
2.54	(368)	3.41	(495)	3.74	(542)	3.88	(562)
2.54	(369)	3.42	(496)	3.74	(542)	3.89	(564)
2.55	(370)	3.44	(499)	3.74	(543)	3.90	(566)
2.59	(375)	3.48	(504)	3.75	(544)	3.93	(570)
2.88	(417)	3.50	(508)	3.76	(545)	3.94	(571)
2.92	(423)	3.53	(512)	3.76	(545)	3.95	(573)
2.96	(429)	3.56	(516)*	3.78	(548)	3.97	(575)
2.97	(431)	3.59	(520)	3.79	(549)	3.98	(577)
3.01	(437)	3.59	(521)	3.79	(550)	4.00	(580)
3.02	(439)	3.59	(521)	3.80	(551)	4.01	(582)
3.03	(440)	3.60	(522)	3.80	(551)	4.01	(582)
3.06	(444)	3.61	(524)	3.80	(551)	4.02	(583)
3.10	(449)	3.62	(525)	3.81	(552)	4.02	(583)
3.11	(451)	3.64	(528)	3.81	(552)	4.03	(584)
3.21	(466)	3.65	(529)	3.81	(552)	4.03	(585)
3.24	(470)	3.65	(530)	3.81	(553)	4.04	(587)
3.31	(480)	3.66	(531)	3.82	(554)	4.05	(588)
3.32	(482)	3.67	(532)	3.82	(554)	4.07	(590)
3.34	(484)	3.67	(532)	3.83	(555)	4.10	(595)
3.35	(486)	3.68	(533)	3.83	(556)	4.14	(600)
3.38	(490)	3.68	(533)	3.83	(556)	4.15	(602)

*Approximate mean value.

TABLE II.- STRENGTHS OF BORON FILAMENTS 0.14 mm (0.0056 in.)

IN DIAMETER RECLAIMED FROM COMPOSITE BATCH 44

Strength, GN/m^2	(ksi)	Strength, GN/m^2	(ksi)	Strength, GN/m^2	(ksi)	Strength, GN/m^2	(ksi)	Strength, GN/m^2	(ksi)	Strength, GN/m^2	(ksi)
1.70	(247)	2.28	(330)	2.41	(349)	2.50	(363)	2.62	(380)	2.72	(394)
1.74	(252)	2.29	(332)	2.41	(350)	2.51	(364)	2.63	(381)	2.72	(394)
1.74	(252)	2.30	(333)	2.42	(351)	2.51	(364)	2.63	(381)	2.73	(396)
1.76	(255)	2.30	(333)	2.43	(352)	2.51	(364)	2.63	(381)	2.74	(397)
1.81	(263)	2.31	(335)	2.43	(352)	2.52	(365)	2.64	(383)	2.74	(397)
1.86	(269)	2.32	(336)	2.43	(353)	2.52	(365)	2.65	(384)	2.74	(398)
1.90	(275)	2.32	(336)	2.43	(353)	2.52	(366)	2.65	(384)	2.74	(398)
1.92	(279)	2.32	(337)	2.44	(354)	2.52	(366)	2.66	(385)	2.75	(399)
2.01	(291)	2.34	(339)	2.44	(354)	2.53	(367)	2.66	(386)	2.75	(399)
2.03	(294)	2.34	(339)	2.44	(354)	2.54	(369)	2.66	(386)	2.75	(399)
2.04	(296)	2.34	(339)	2.44	(354)	2.54	(369)	2.66	(386)	2.76	(400)
2.12	(308)	2.34	(340)	2.45	(355)	2.55	(370)	2.66	(386)	2.77	(402)
2.13	(310)	2.34	(340)	2.45	(355)	2.55	(370)	2.67	(387)	2.77	(402)
2.14	(311)	2.34	(340)	2.46	(356)	2.55	(370)	2.67	(387)	2.77	(402)
2.17	(315)	2.35	(341)	2.46	(356)	2.56	(371)	2.68	(388)	2.78	(403)
2.20	(319)	2.35	(341)	2.46	(357)*	2.57	(373)	2.68	(388)	2.78	(403)
2.21	(321)	2.37	(343)	2.46	(357)	2.58	(374)	2.68	(389)	2.78	(403)
2.23	(322)	2.37	(343)	2.48	(359)	2.59	(375)	2.68	(389)	2.80	(406)
2.25	(326)	2.38	(345)	2.48	(359)	2.59	(375)	2.69	(390)	2.81	(407)
2.25	(326)	2.38	(345)	2.49	(361)	2.59	(375)	2.70	(391)	2.81	(408)
2.26	(327)	2.38	(345)	2.49	(361)	2.59	(375)	2.70	(391)	2.81	(408)
2.26	(328)	2.39	(347)	2.49	(361)	2.60	(377)	2.70	(391)	2.83	(410)
2.26	(328)	2.39	(347)	2.49	(361)	2.61	(379)	2.70	(392)	2.85	(413)
2.28	(330)	2.40	(348)	2.50	(362)	2.61	(379)	2.70	(392)	2.89	(419)
2.28	(330)	2.40	(348)	2.50	(362)	2.61	(379)	2.70	(392)	2.94	(427)

*Approximate mean value.

TABLE III.- AVERAGE FILAMENT STRESSES AT COMPOSITE FAILURE FOR COMPOSITE BATCHES 44 AND 47 TO 51, COMMERCIALLY FABRICATED COMPOSITES, AND WEAKLY BONDED COMPOSITE

Average filament stress at composite failure, GN/m^2 (ksi), for –								
Batch 44	Batch 47	Batch 48	Batch 49	Batch 50	Batch 51	Commercially fabricated, five-layer	Commercially fabricated, monolayer	Weakly bonded
1.52 (220)	1.14 (165)	0.99 (143)	0.88 (127)	0.95 (138)	0.91 (132)	0.83 (120)	2.38 (346)	1.03 (150)
1.56 (226)	1.18 (171)	1.02 (149)	.91 (132)	.99 (143)	.95 (138)	1.04 (151)	2.43 (352)	1.10 (160)
1.59 (231)	1.18 (171)	1.06 (154)	1.06 (154)	1.03 (149)	.95 (138)	1.10 (160)	2.48 (359)	1.10 (160)
1.59 (231)	1.18 (171)	1.06 (154)	1.14 (165)	1.06 (154)	.99 (143)	1.18 (171)*	2.51 (364)	1.10 (160)
1.59 (231)	1.18 (171)	1.17 (170)	1.14 (165)	1.06 (154)	.99 (143)	1.23 (179)	2.54 (368)	1.14 (165)
1.63 (237)	1.21 (176)	1.18 (171)*	1.18 (171)*	1.06 (154)	.99 (143)	1.38 (200)	2.54 (368)	1.14 (165)
1.67 (242)	1.21 (176)	1.18 (171)	1.21 (176)	1.14 (165)	1.03 (149)		2.54 (368)	1.18 (171)
1.67 (242)	1.26 (182)	1.18 (171)	1.29 (187)	1.18 (171)*	1.03 (149)		2.54 (368)	1.18 (171)
1.67 (242)	1.26 (182)	1.18 (171)	1.29 (187)	1.18 (171)	1.06 (154)*		2.71 (393)*	1.18 (171)
1.67 (242)	1.29 (187)	1.26 (182)	1.37 (198)	1.18 (171)	1.14 (165)		2.72 (394)	1.18 (171)
1.71 (248)*	1.29 (187)	1.28 (186)	1.41 (204)	1.21 (176)	1.26 (182)		2.78 (403)	1.21 (176)*
1.79 (259)	1.33 (193)*	1.60 (232)	1.44 (209)	1.29 (187)	1.33 (193)		2.84 (411)	1.21 (176)
1.82 (264)	1.33 (193)			1.33 (193)			2.84 (412)	1.26 (182)
1.90 (275)	1.33 (193)			1.37 (198)			2.87 (416)	1.26 (182)
2.01 (292)	1.37 (198)			1.44 (209)			2.98 (432)	1.29 (187)
	1.44 (209)			1.59 (231)				1.37 (198)
	1.48 (215)							1.48 (215)
	1.56 (226)							1.55 (225)
	1.56 (226)							
	1.59 (231)							

*Approximate mean value.

TABLE IV.- STRENGTHS OF VIRGIN BORON FILAMENTS

0.099 mm (0.0039 in.) IN DIAMETER

Strength, GN/m^2	(ksi)	Strength, GN/m^2	(ksi)	Strength, GN/m^2	(ksi)	Strength, GN/m^2	(ksi)	Strength, GN/m^2	(ksi)	Strength, GN/m^2	(ksi)
2.32	(336)	3.48	(504)	3.63	(527)	3.74	(542)	3.79	(549)	3.87	(561)
2.48	(359)	3.48	(504)	3.63	(527)	3.74	(542)	3.79	(550)	3.88	(562)
2.57	(372)	3.49	(506)	3.64	(528)	3.74	(542)	3.79	(550)	3.88	(562)
2.74	(398)	3.49	(506)	3.64	(528)	3.74	(543)	3.79	(550)	3.88	(562)
2.98	(432)	3.50	(508)	3.65	(529)	3.74	(543)	3.81	(552)	3.88	(562)
2.98	(432)	3.52	(510)	3.65	(529)	3.74	(543)	3.81	(553)	3.88	(562)
2.99	(433)	3.53	(512)	3.65	(530)*	3.75	(544)	3.81	(553)	3.88	(563)
3.07	(445)	3.54	(514)	3.66	(531)	3.75	(544)	3.81	(553)	3.88	(563)
3.08	(447)	3.56	(516)	3.66	(531)	3.76	(545)	3.81	(553)	3.89	(564)
3.12	(453)	3.57	(517)	3.68	(533)	3.76	(545)	3.81	(553)	3.89	(564)
3.23	(468)	3.57	(518)	3.68	(533)	3.76	(545)	3.81	(553)	3.89	(564)
3.28	(476)	3.59	(520)	3.68	(534)	3.76	(545)	3.82	(554)	3.89	(564)
3.31	(480)	3.59	(521)	3.69	(535)	3.76	(545)	3.82	(554)	3.90	(565)
3.34	(485)	3.60	(522)	3.69	(535)	3.76	(545)	3.82	(554)	3.90	(565)
3.39	(492)	3.61	(523)	3.69	(535)	3.76	(545)	3.82	(554)	3.90	(566)
3.40	(493)	3.61	(523)	3.70	(536)	3.77	(546)	3.83	(555)	3.91	(567)
3.41	(494)	3.61	(523)	3.70	(536)	3.77	(546)	3.83	(556)	3.92	(569)
3.41	(495)	3.61	(523)	3.70	(536)	3.77	(546)	3.83	(556)	3.92	(569)
3.41	(495)	3.61	(524)	3.70	(537)	3.77	(546)	3.84	(557)	3.93	(570)
3.41	(495)	3.61	(524)	3.70	(537)	3.77	(546)	3.84	(557)	3.93	(570)
3.43	(497)	3.61	(524)	3.71	(538)	3.77	(546)	3.85	(558)	3.95	(573)
3.44	(499)	3.62	(525)	3.71	(538)	3.77	(547)	3.86	(560)	3.98	(577)
3.45	(501)	3.62	(525)	3.72	(539)	3.77	(547)	3.86	(560)	3.99	(578)
3.46	(502)	3.63	(526)	3.72	(539)	3.77	(547)	3.87	(561)	3.99	(579)
3.48	(504)	3.63	(527)	3.73	(541)	3.79	(549)	3.87	(561)	4.19	(608)
				3.74	(542)	3.79	(549)				

*Approximate mean value.

TABLE V.- STRENGTHS OF BORON FILAMENTS 0.099 mm (0.0039 in.) IN DIAMETER RECLAIMED FROM COMPOSITE BATCH 47

Strength, GN/m^2	(ksi)	Strength, GN/m^2	(ksi)	Strength, GN/m^2	(ksi)	Strength, GN/m^2	(ksi)
1.32	(191)	1.91	(277)	2.14	(311)	2.28	(331)
1.33	(193)	1.92	(278)	2.15	(312)	2.28	(331)
1.45	(210)	1.92	(279)	2.15	(312)	2.31	(335)
1.55	(225)	1.94	(281)	2.15	(312)	2.34	(339)
1.71	(248)	1.95	(283)	2.15	(312)	2.34	(339)
1.74	(252)	1.95	(283)	2.15	(312)	2.34	(340)
1.74	(252)	1.96	(284)	2.16	(313)	2.35	(341)
1.74	(253)	1.96	(284)	2.16	(313)	2.35	(341)
1.76	(255)	1.96	(284)	2.17	(314)	2.35	(341)
1.77	(257)	1.97	(286)	2.19	(317)	2.35	(341)
1.79	(259)	1.99	(289)	2.19	(318)	2.36	(342)
1.79	(259)	2.00	(290)	2.19	(318)	2.37	(343)
1.79	(260)	2.02	(293)	2.20	(319)	2.37	(343)
1.81	(263)	2.02	(293)	2.20	(319)	2.38	(345)
1.82	(264)	2.02	(293)	2.21	(321)	2.38	(345)
1.83	(265)	2.03	(294)	2.22	(322)	2.39	(346)
1.83	(265)	2.03	(295)	2.23	(323)	2.39	(346)
1.86	(270)	2.06	(298)	2.23	(323)	2.41	(349)
1.86	(270)	2.06	(299)	2.23	(324)	2.42	(351)
1.86	(270)	2.06	(299)	2.24	(325)	2.42	(351)
1.88	(272)	2.07	(300)	2.25	(326)	2.42	(351)
1.88	(273)	2.07	(300)	2.26	(327)	2.42	(351)
1.89	(274)	2.08	(302)*	2.26	(327)	2.54	(369)
1.89	(274)	2.10	(304)	2.26	(327)	2.66	(385)
1.90	(276)	2.10	(305)	2.27	(329)	2.70	(392)

*Approximate mean value.

TABLE VI. - STRENGTHS OF BORON FILAMENTS 0.099 mm (0.0039 in.) IN DIAMETER RECLAIMED FROM COMPOSITE BATCH 48

Strength, GN/m^2	(ksi)	Strength, GN/m^2	(ksi)	Strength, GN/m^2	(ksi)	Strength, GN/m^2	(ksi)
0.56	(81)	1.77	(257)	1.99	(289)	2.16	(313)
.67	(97)	1.79	(259)	1.99	(289)	2.17	(315)
.77	(111)	1.79	(260)	2.00	(290)	2.18	(316)
.85	(123)	1.79	(260)	2.00	(290)	2.19	(317)
1.01	(147)	1.81	(262)	2.00	(290)	2.19	(317)
1.08	(156)	1.81	(263)	2.01	(291)	2.20	(319)
1.10	(159)	1.85	(268)	2.01	(291)	2.23	(323)
1.13	(164)	1.86	(270)	2.02	(293)	2.23	(324)
1.19	(172)	1.86	(270)	2.03	(294)	2.23	(324)
1.28	(186)	1.88	(273)	2.03	(294)	2.23	(324)
1.36	(197)	1.89	(274)	2.03	(294)	2.26	(327)
1.40	(203)	1.90	(276)*	2.05	(297)	2.27	(329)
1.40	(203)	1.90	(276)	2.06	(298)	2.28	(331)
1.44	(209)	1.93	(280)	2.07	(300)	2.28	(331)
1.52	(221)	1.94	(282)	2.07	(300)	2.28	(331)
1.64	(238)	1.94	(282)	2.08	(302)	2.28	(331)
1.65	(239)	1.95	(283)	2.10	(304)	2.32	(336)
1.66	(241)	1.95	(283)	2.10	(305)	2.33	(338)
1.70	(246)	1.96	(284)	2.12	(307)	2.33	(338)
1.70	(247)	1.96	(284)	2.12	(307)	2.39	(346)
1.72	(250)	1.96	(284)	2.12	(308)	2.40	(348)
1.73	(251)	1.97	(286)	2.13	(309)	2.44	(354)
1.74	(253)	1.98	(287)	2.15	(312)	2.53	(367)
1.74	(253)	1.98	(287)	2.15	(312)	2.60	(377)
1.74	(253)	1.99	(289)	2.16	(313)	2.63	(381)

*Approximate mean value.

TABLE VII.- STRENGTHS OF BORON FILAMENTS 0.099 mm (0.0039 in.) IN DIAMETER RECLAIMED FROM COMPOSITE BATCH 49

Strength, GN/m^2	(ksi)	Strength, GN/m^2	(ksi)	Strength, GN/m^2	(ksi)	Strength, GN/m^2	(ksi)
0.29	(42)	1.34	(194)	2.06	(299)	2.22	(322)
.47	(68)	1.36	(197)	2.06	(299)	2.22	(322)
.50	(73)	1.57	(228)	2.07	(300)	2.23	(324)
.55	(80)	1.64	(238)	2.07	(300)	2.24	(325)
.58	(84)	1.64	(238)	2.08	(301)	2.26	(327)
.59	(86)	1.65	(239)	2.09	(303)	2.26	(327)
.61	(88)	1.69	(245)	2.10	(304)	2.26	(327)
.62	(90)	1.79	(260)*	2.10	(304)	2.28	(331)
.63	(92)	1.86	(269)	2.10	(305)	2.29	(332)
.66	(95)	1.86	(270)	2.10	(305)	2.30	(333)
.70	(101)	1.92	(278)	2.11	(306)	2.30	(333)
.70	(101)	1.93	(280)	2.12	(308)	2.30	(333)
.72	(104)	1.93	(280)	2.14	(311)	2.30	(334)
.72	(105)	1.97	(285)	2.14	(311)	2.31	(335)
.79	(115)	1.97	(285)	2.14	(311)	2.32	(336)
.81	(118)	1.99	(289)	2.15	(312)	2.32	(336)
.83	(121)	1.99	(289)	2.16	(313)	2.32	(336)
.92	(133)	2.00	(290)	2.17	(315)	2.34	(340)
.93	(135)	2.00	(290)	2.18	(316)	2.35	(341)
.96	(139)	2.01	(291)	2.18	(316)	2.35	(341)
.99	(143)	2.02	(293)	2.19	(317)	2.35	(341)
1.09	(158)	2.02	(293)	2.19	(318)	2.37	(344)
1.11	(161)	2.03	(294)	2.21	(320)	2.37	(344)
1.26	(183)	2.06	(298)	2.21	(320)	2.41	(350)
1.30	(189)	2.06	(298)	2.21	(321)	2.44	(354)

*Approximate mean value.

TABLE VIII. - STRENGTHS OF BORON FILAMENTS 0.099 mm (0.0039 in.) IN DIAMETER RECLAIMED FROM COMPOSITE BATCH 50

Strength, GN/m^2	(ksi)	Strength, GN/m^2	(ksi)	Strength, GN/m^2	(ksi)	Strength, GN/m^2	(ksi)
0.30	(43)	1.26	(183)	1.71	(248)	1.94	(281)
.36	(52)	1.27	(184)	1.71	(248)	1.94	(281)
.44	(64)	1.28	(185)	1.72	(250)	1.94	(282)
.44	(64)	1.30	(189)	1.73	(251)	1.95	(283)
.44	(64)	1.39	(202)	1.74	(252)	1.96	(284)
.48	(70)	1.41	(205)	1.78	(258)	1.96	(284)
.50	(73)	1.42	(206)	1.79	(258)	1.97	(286)
.61	(88)	1.46	(212)	1.79	(259)	1.97	(286)
.63	(92)	1.50	(218)	1.79	(259)	1.98	(287)
.64	(93)	1.52	(221)	1.79	(260)	1.98	(287)
.73	(106)	1.54	(223)*	1.81	(262)	2.01	(292)
.76	(110)	1.54	(224)	1.87	(264)	2.02	(293)
.77	(111)	1.54	(224)	1.84	(267)	2.07	(300)
.79	(115)	1.55	(225)	1.84	(267)	2.08	(302)
.80	(116)	1.56	(226)	1.85	(268)	2.09	(303)
.84	(122)	1.56	(226)	1.86	(270)	2.10	(304)
.88	(127)	1.57	(227)	1.88	(273)	2.12	(308)
.88	(127)	1.57	(227)	1.88	(273)	2.14	(310)
.91	(132)	1.63	(237)	1.88	(273)	2.14	(311)
.93	(135)	1.63	(237)	1.91	(277)	2.15	(312)
1.03	(150)	1.67	(242)	1.91	(277)	2.30	(333)
1.12	(162)	1.67	(242)	1.91	(277)	2.31	(335)
1.21	(176)	1.68	(243)	1.92	(278)	2.46	(356)
1.23	(179)	1.68	(243)	1.92	(278)	2.46	(357)
1.26	(182)	1.68	(243)	1.92	(279)	2.50	(362)
		1.68	(244)	1.92	(279)		

*Approximate mean value.

TABLE IX. - STRENGTHS OF BORON FILAMENTS 0.099 mm (0.0039 in.) IN DIAMETER RECLAIMED FROM COMPOSITE BATCH 51

Strength, GN/m^2	(ksi)	Strength, GN/m^2	(ksi)	Strength, GN/m^2	(ksi)	Strength, GN/m^2	(ksi)
0.12	(18)	0.62	(90)	1.90	(275)	2.63	(381)
.17	(24)	.63	(92)	1.91	(277)	2.63	(381)
.19	(28)	.64	(93)	2.06	(299)	2.63	(382)
.22	(32)	.66	(96)	2.09	(303)	2.66	(385)
.22	(32)	.67	(97)	2.24	(325)	2.66	(386)
.28	(40)	.68	(98)	2.26	(327)	2.68	(388)
.29	(42)	.69	(100)	2.38	(345)	2.68	(388)
.34	(49)	.72	(105)	2.41	(350)	2.68	(389)
.37	(54)	.78	(113)	2.46	(356)	2.70	(391)
.39	(57)	.79	(114)	2.48	(360)	2.70	(392)
.40	(58)	.79	(115)	2.48	(360)	2.70	(392)
.43	(63)	.84	(122)	2.50	(363)	2.72	(395)
.44	(64)	.85	(123)	2.54	(368)	2.73	(396)
.44	(64)	.86	(124)	2.54	(369)	2.73	(396)
.44	(64)	.90	(130)	2.55	(370)	2.74	(397)
.48	(69)	.92	(133)	2.55	(370)	2.74	(397)
.48	(70)	.93	(135)	2.56	(371)	2.74	(397)
.49	(71)	.96	(139)	2.57	(372)	2.74	(397)
.53	(77)	.97	(140)	2.59	(375)	2.74	(398)
.55	(80)	1.01	(147)	2.60	(377)	2.74	(398)
.58	(84)	1.45	(210)	2.60	(377)	2.75	(399)
.59	(85)	1.66	(240)*	2.61	(378)	2.77	(401)
.59	(86)	1.82	(264)	2.61	(379)	2.77	(401)
.60	(87)	1.83	(265)	2.61	(379)	2.77	(402)
.61	(89)	1.85	(268)	2.62	(380)	2.78	(403)

*Approximate mean value.

TABLE X.- STRENGTHS OF BORON FILAMENTS 0.089 mm (0.0035 in.) IN DIAMETER RECLAIMED FROM WEAKLY BONDED COMPOSITE

Strength, GN/m^2	(ksi)	Strength, GN/m^2	(ksi)	Strength, GN/m^2	(ksi)	Strength, GN/m^2	(ksi)
0.38	(55)	1.50	(218)	1.63	(237)	2.27	(329)
.39	(56)	1.51	(219)	1.63	(237)	2.36	(342)
.39	(57)	1.52	(220)	1.63	(237)	2.43	(353)
.40	(58)	1.52	(221)	1.64	(238)	2.49	(361)
.50	(72)	1.53	(222)	1.65	(239)	2.52	(365)
.51	(74)	1.54	(224)	1.65	(239)	2.53	(367)
.69	(100)	1.55	(225)	1.66	(240)	2.66	(385)
.77	(112)	1.56	(226)	1.66	(240)	2.71	(393)
.84	(122)	1.57	(227)	1.67	(242)	2.72	(395)
.88	(128)	1.57	(228)	1.68	(243)	2.76	(400)
.93	(135)	1.58	(229)	1.68	(244)	2.78	(403)
.93	(135)	1.58	(229)	1.69	(245)	2.79	(405)
.94	(136)	1.59	(230)	1.69	(245)	2.88	(418)
.97	(141)	1.59	(230)	1.69	(245)	2.97	(431)
1.01	(146)	1.59	(230)	1.70	(246)	3.14	(456)
1.01	(147)	1.59	(230)	1.70	(247)	3.27	(474)
1.09	(158)	1.59	(231)	1.72	(249)	3.40	(493)
1.12	(162)	1.59	(231)	1.72	(250)	3.54	(513)
1.12	(162)	1.59	(231)	1.74	(252)	3.83	(556)
1.21	(176)	1.60	(232)	1.76	(255)	4.03	(585)
1.39	(201)	1.60	(232)	1.79	(260)	4.15	(602)
1.43	(208)	1.61	(233)	1.90	(275)*	4.35	(631)
1.48	(214)	1.61	(234)	2.00	(290)	4.45	(646)
1.49	(216)	1.62	(235)	2.10	(305)	4.49	(651)
1.50	(218)	1.63	(236)	2.17	(315)	4.50	(652)

*Approximate mean value.

TABLE XI. - STRENGTHS OF 0.10-mm-DIAMETER (0.0041-in.) SILICON-CARBIDE-COATED BORON FILAMENT RECLAIMED FROM COMMERCIALLY FABRICATED COMPOSITE

Strength, GN/m^2	(ksi)	Strength, GN/m^2	(ksi)	Strength, GN/m^2	(ksi)	Strength, GN/m^2	(ksi)
0.32	(46)	1.05	(152)	2.41	(350)	3.10	(449)
.34	(49)	1.08	(156)	2.58	(374)	3.13	(454)
.42	(61)	1.22	(177)	2.61	(379)	3.13	(454)
.43	(62)	1.35	(195)	2.61	(379)	3.16	(458)
.44	(64)	1.37	(199)	2.62	(380)	3.17	(459)
.46	(67)	1.38	(200)	2.66	(386)	3.20	(464)
.50	(73)	1.43	(207)	2.66	(386)	3.21	(465)
.52	(76)	1.46	(212)	2.72	(394)	3.22	(467)
.55	(80)	1.49	(216)	2.77	(402)	3.22	(467)
.59	(85)	1.55	(225)	2.80	(406)	3.23	(468)
.63	(92)	1.57	(227)	2.82	(409)	3.23	(469)
.66	(96)	1.57	(227)	2.86	(415)	3.24	(470)
.68	(98)	1.63	(236)	2.89	(419)	3.25	(471)
.70	(101)	1.63	(237)	2.93	(425)	3.26	(473)
.70	(101)	1.70	(246)	2.94	(427)	3.28	(475)
.77	(111)	1.74	(253)	2.94	(427)	3.28	(476)
.77	(111)	1.90	(275)	2.97	(430)	3.28	(476)
.83	(120)	1.91	(277)	2.98	(432)	3.32	(482)
.95	(137)	1.93	(280)	2.99	(433)	3.33	(483)
.96	(139)	1.95	(283)	2.99	(434)	3.33	(483)
.96	(139)	2.04	(296)	3.03	(439)	3.34	(485)
.96	(139)	2.12	(307)*	3.05	(442)	3.38	(490)
.98	(142)	2.21	(321)	3.08	(447)	3.39	(491)
.99	(143)	2.23	(324)	3.09	(448)	3.41	(494)
1.01	(147)	2.31	(335)	3.10	(449)	3.41	(495)
						3.42	(496)

*Approximate mean value.

TABLE XII. - STRENGTHS OF BORON FILAMENTS 0.14 mm (0.0056 in.) IN DIAMETER RECLAIMED FROM COMMERCIALLY FABRICATED COMPOSITE

Strength, GN/m^2	(ksi)	Strength, GN/m^2	(ksi)	Strength, GN/m^2	(ksi)	Strength, GN/m^2	(ksi)	Strength, GN/m^2	(ksi)
2.60	(377)	3.61	(523)	3.81	(552)	3.97	(576)	4.08	(592)
2.61	(378)	3.61	(524)	3.83	(555)	3.97	(576)	4.08	(592)
2.66	(386)	3.61	(524)	3.83	(555)	3.97	(576)	4.08	(592)
2.72	(395)	3.61	(524)	3.86	(560)	4.00	(580)	4.08	(592)
2.80	(406)	3.63	(527)	3.86	(560)	4.00	(580)	4.08	(592)
2.85	(414)	3.67	(532)	3.89	(564)	4.00	(580)	4.08	(592)
2.88	(418)	3.69	(535)	3.89	(564)	4.00	(580)	4.09	(593)
2.96	(430)	3.69	(535)	3.92	(568)	4.00	(580)	4.11	(596)
2.96	(430)	3.69	(535)	3.92	(568)	4.00	(580)	4.11	(596)
2.99	(434)	3.70	(536)	3.92	(568)	4.00	(580)	4.11	(596)
3.02	(438)	3.72	(539)	3.92	(568)	4.00	(580)	4.12	(597)
3.21	(466)	3.72	(539)	3.92	(568)	4.01	(581)	4.14	(600)
3.24	(470)	3.72	(539)	3.92	(568)	4.01	(581)	4.14	(600)
3.25	(471)	3.72	(539)	3.92	(568)	4.01	(581)	4.16	(604)
3.39	(491)	3.72	(539)	3.92	(568)	4.01	(581)	4.16	(604)
3.39	(491)	3.72	(540)	3.94	(572)	4.03	(584)	4.16	(604)
3.41	(495)	3.74	(543)	3.94	(572)	4.03	(584)	4.19	(608)
3.47	(503)	3.74	(543)	3.94	(572)	4.03	(584)	4.19	(608)
3.47	(503)	3.74	(543)	3.97	(576)	4.03	(584)	4.19	(608)
3.47	(503)	3.74	(543)	3.97	(576)	4.05	(588)	4.25	(616)
3.50	(507)	3.75	(544)	3.97	(576)	4.05	(588)	4.25	(617)
3.52	(511)	3.77	(547)	3.97	(576)	4.06	(589)	4.27	(620)
3.52	(511)	3.77	(547)	3.97	(576)	4.06	(589)	4.28	(621)
3.52	(511)	3.80	(551)*	3.97	(576)	4.06	(589)	4.31	(625)
3.61	(523)	3.80	(551)	3.97	(576)	4.08	(592)	4.36	(633)

*Approximate mean value.

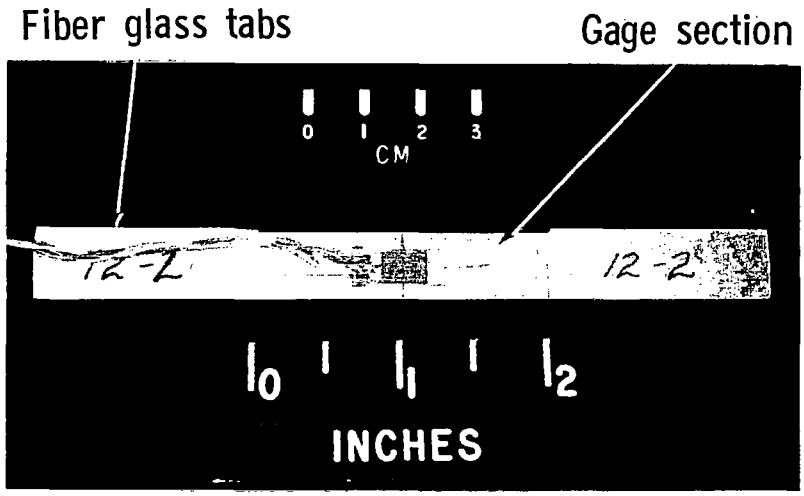

L-72-146

Figure 1.- Typical B-Al sheet tensile specimen prior to testing.

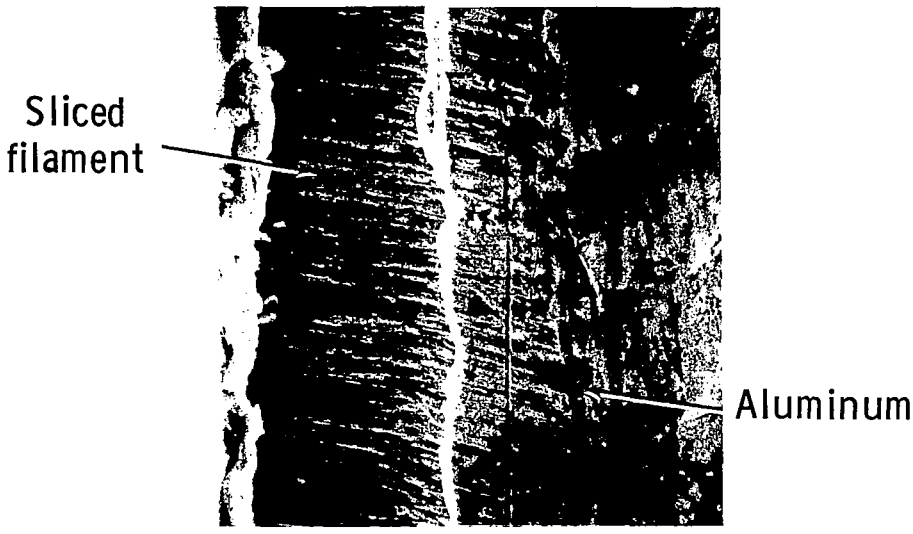

L-72-147

Figure 2.- Edge of bilayer B-Al composite tensile specimen cut by electrical-discharge method.

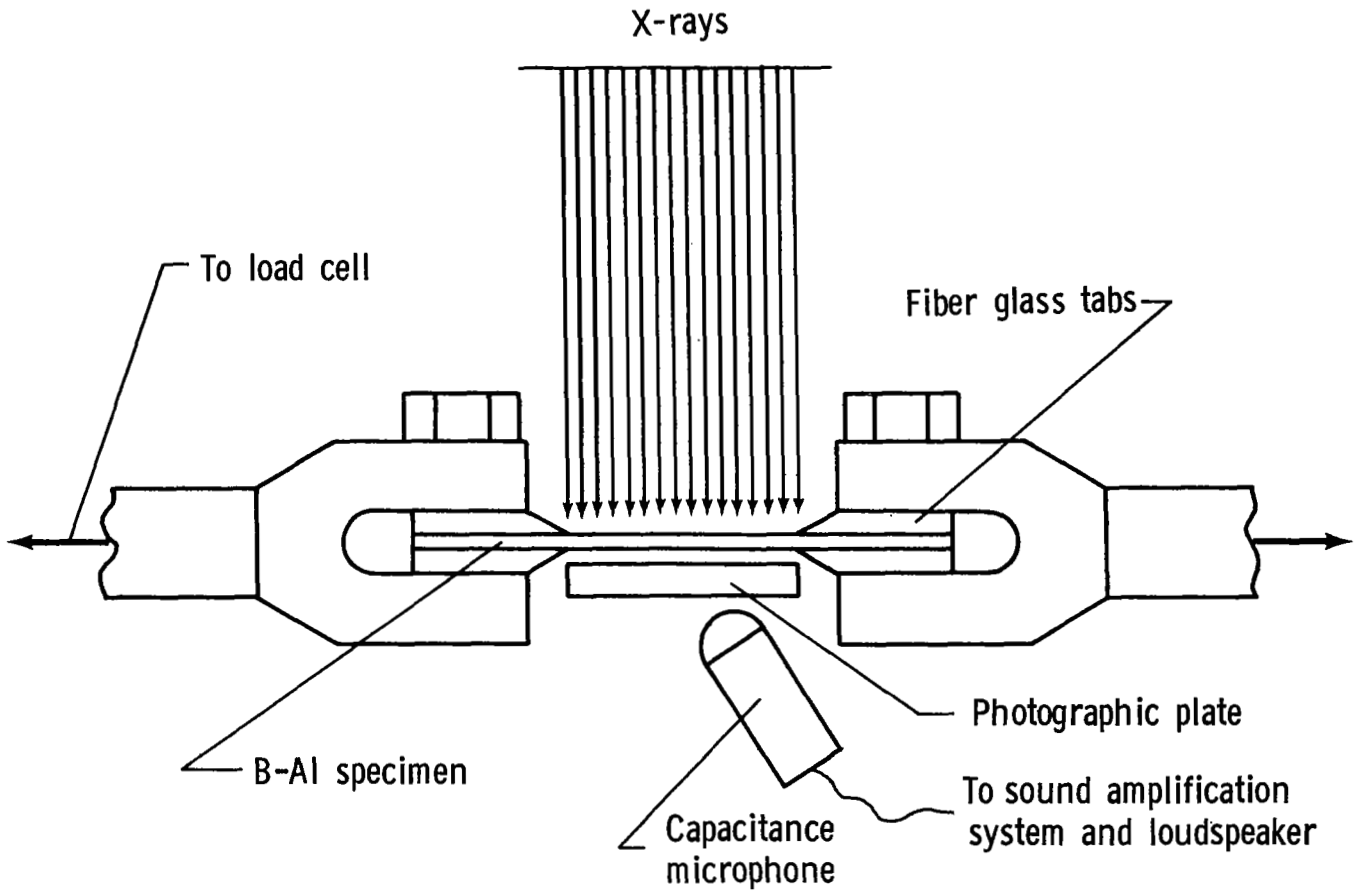

Figure 3.- Schematic drawing of apparatus used to study tensile fracture of B-Al composite sheet.

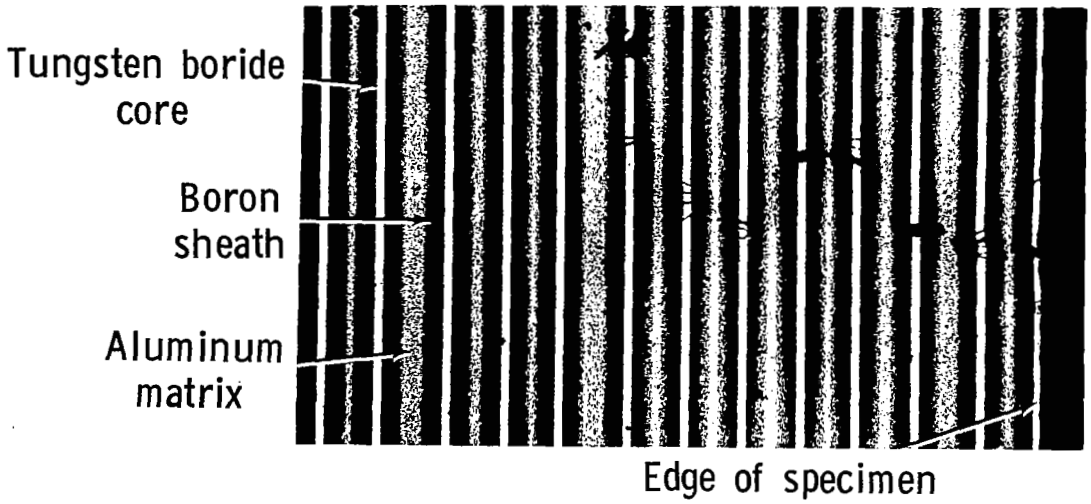

(a) Crack initiation near edge of specimen.

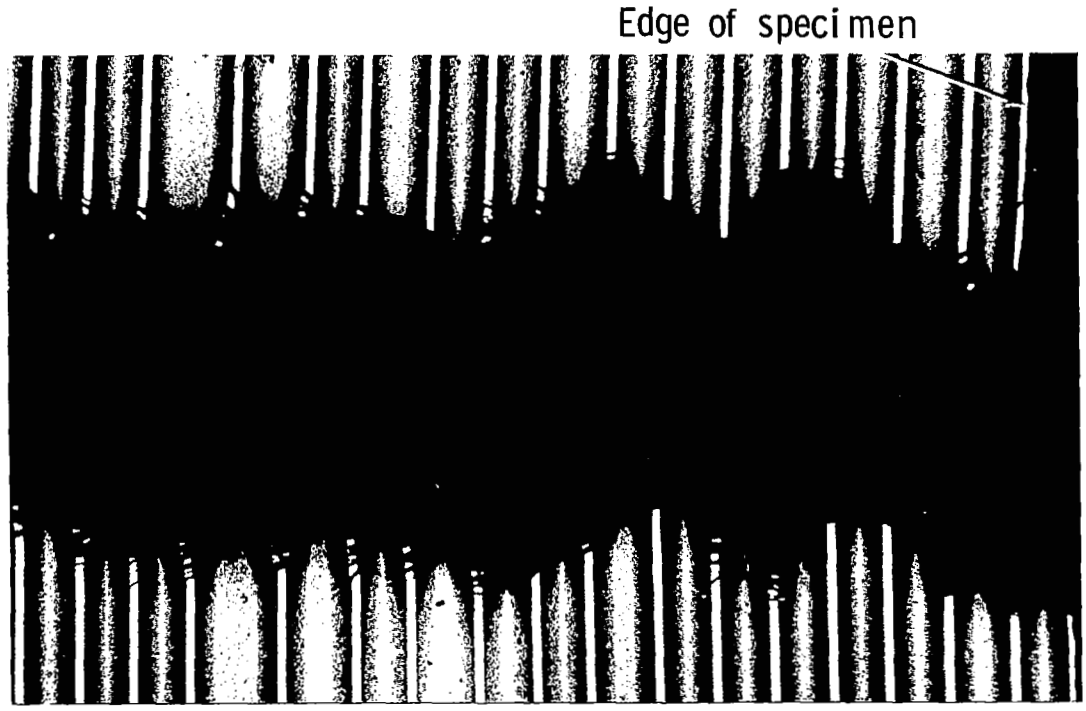

L-72-148

(b) Same region after complete fracture.

Figure 4.- Tensile fractoradiographs of monolayer B-Al composite. Core diameter, 0.015 mm (0.0006 in.).

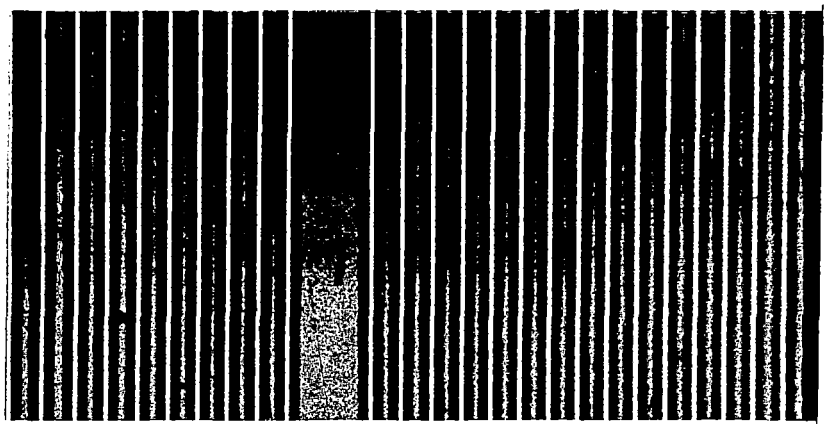

(a) Crack initiation near edge of specimen.

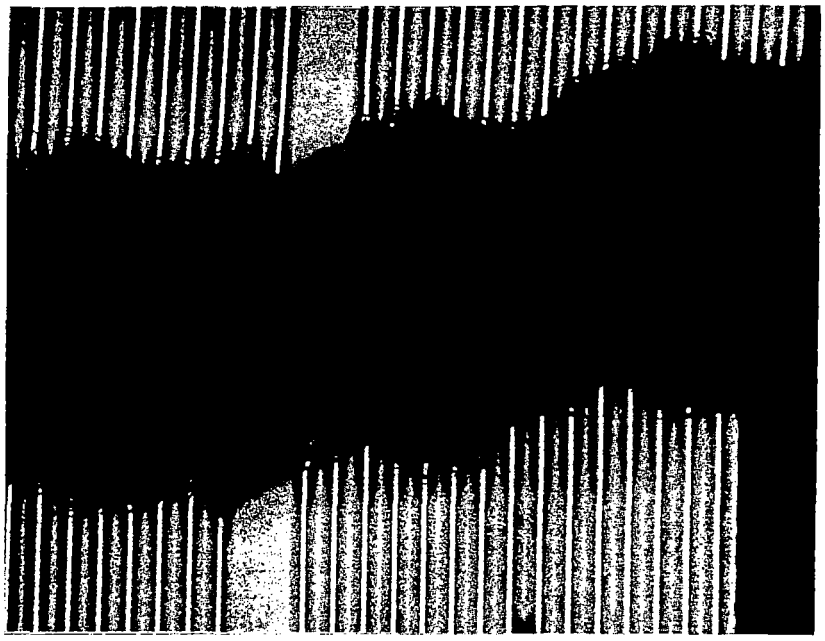

L-72-149

(b) Same region after complete fracture.

Figure 5.- Tensile fractoradiographs of monolayer B-Al composite with missing filaments. Core diameter, 0.015 mm (0.0006 in.).

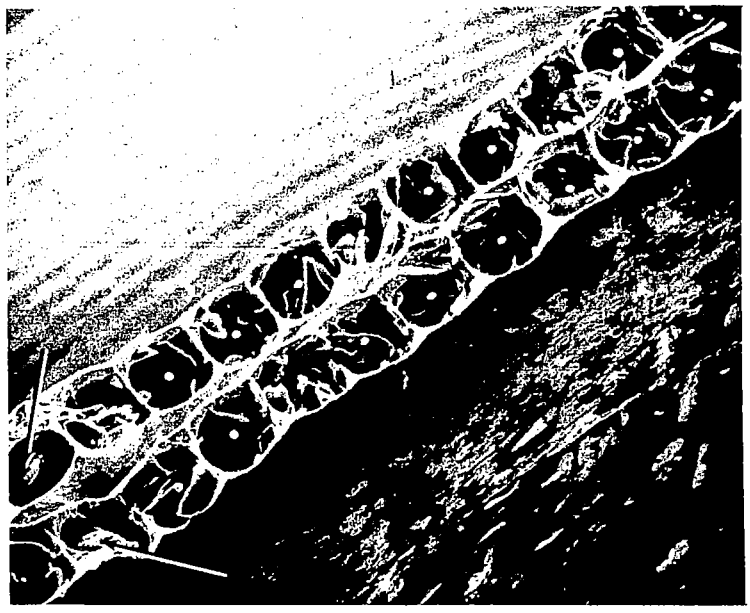

L-72-150

Figure 6.- General view of matching transverse fracture surfaces of monolayer B-Al composite showing filament fragmentation. Filament diameter, 0.14 mm (0.0056 in.).

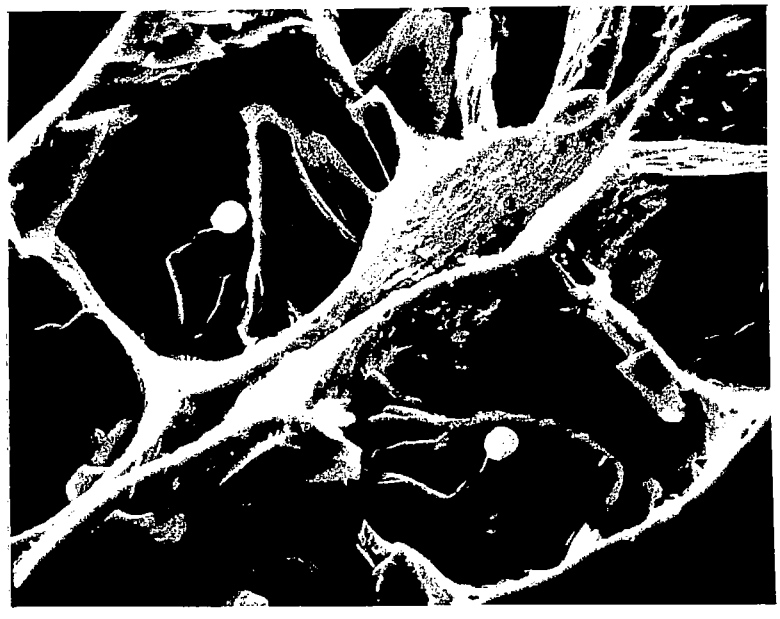

L-72-151

Figure 7.- Matching transverse fracture surfaces of monolayer B-Al composite showing details of matrix fracture. Filament diameter, 0.14 mm (0.0056 in.).

Edge of specimen

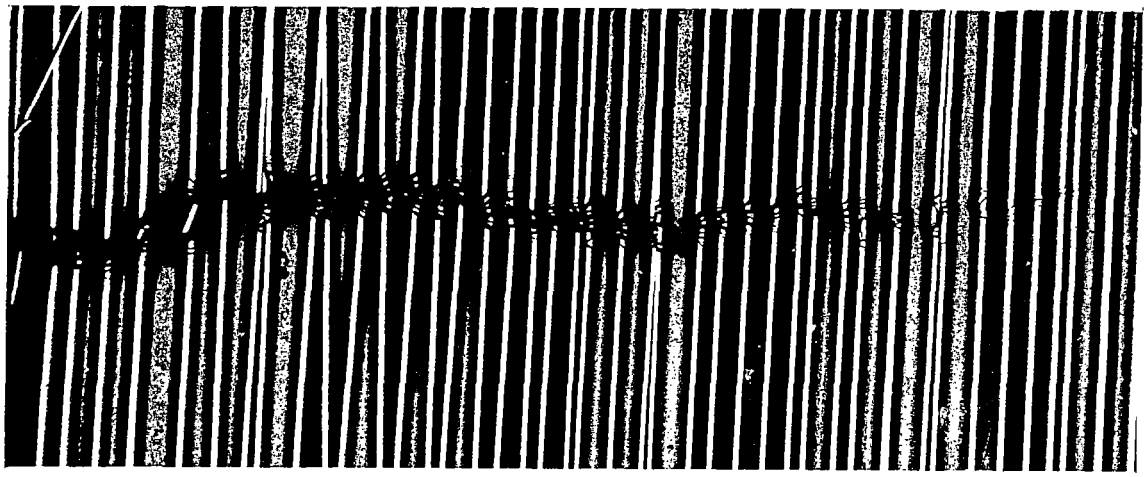

L-72-152

Figure 8.- Fractoradiograph showing arrested crack in bilayer B-Al composite. Core diameter, 0.015 mm (0.0006 in.).

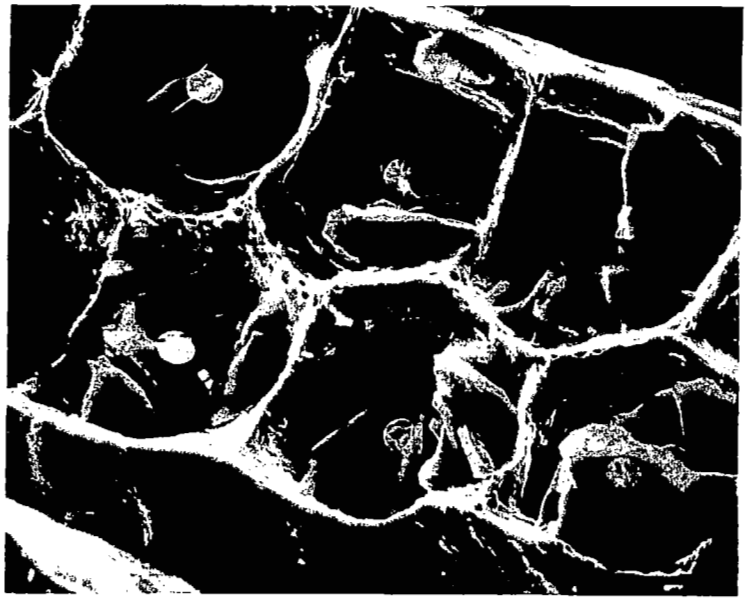

L-72-153

Figure 9.- General view of transverse fracture surface of bilayer B-Al composite showing filament fragmentation. Filament diameter, 0.099 mm (0.0039 in.).

L-72-154

Figure 10.- Transverse fracture surface of bilayer B-Al composite showing details of matrix fracture. Filament diameter, 0.099 mm (0.0039 in.).

L-72-155

Figure 11.- Typical boron filament fragments in a transverse noncumulative fracture surface. Filament diameter, 0.099 mm (0.0039 in.).

L-72-156

Figure 12.- Filament-matrix and matrix-matrix separation in transverse noncumulative fracture surface. Filament diameter, 0.099 mm (0.0039 in.).

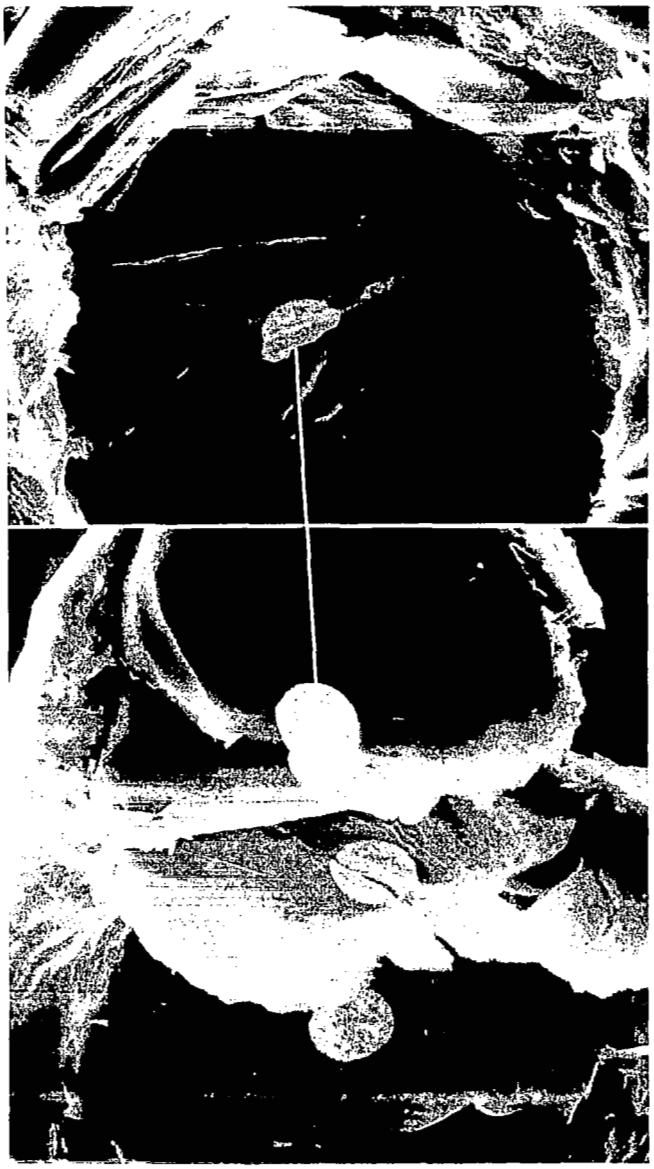

L-72-157

Figure 13.- Matching boron filament fragments from mating transverse noncumulative fracture surfaces. Filament diameter, 0.099 mm (0.0039 in.).

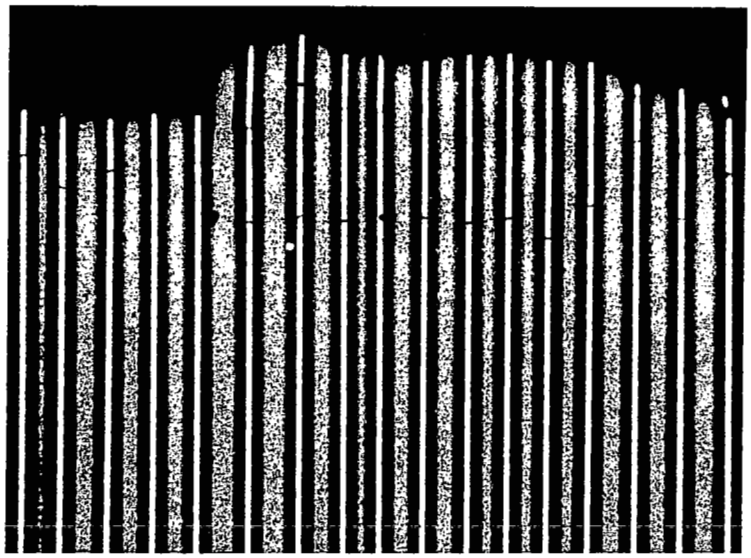

L-72-158

Figure 14.- Fractoradiograph showing rare transverse noncumulative fracture without wedge-shaped fragments. Core diameter, 0.015 mm (0.0006 in.).

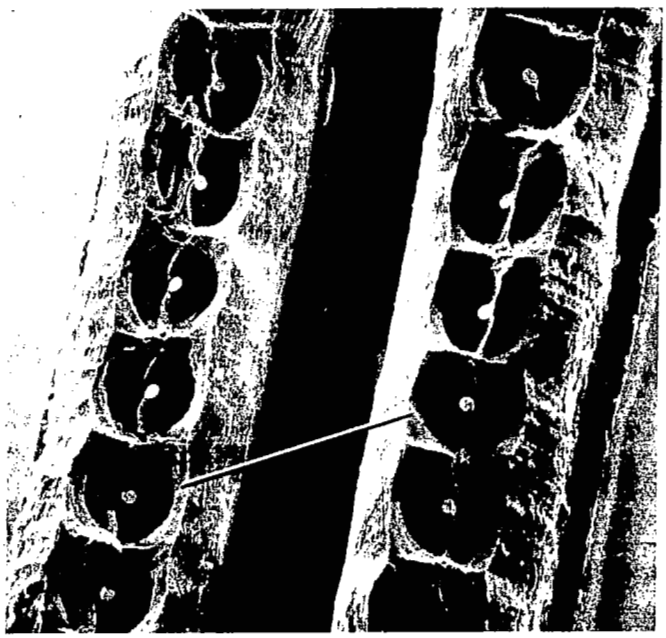

L-72-159

Figure 15.- Matching transverse fracture surfaces of monolayer B-Al composite showing filaments split instead of fragmented. Filament diameter, 0.099 mm (0.0039 in.).

L-72-160

Figure 16.- Fractoradiograph of bilayer B-Al composite exhibiting axial fracture. Core diameter, 0.015 mm (0.0006 in.).

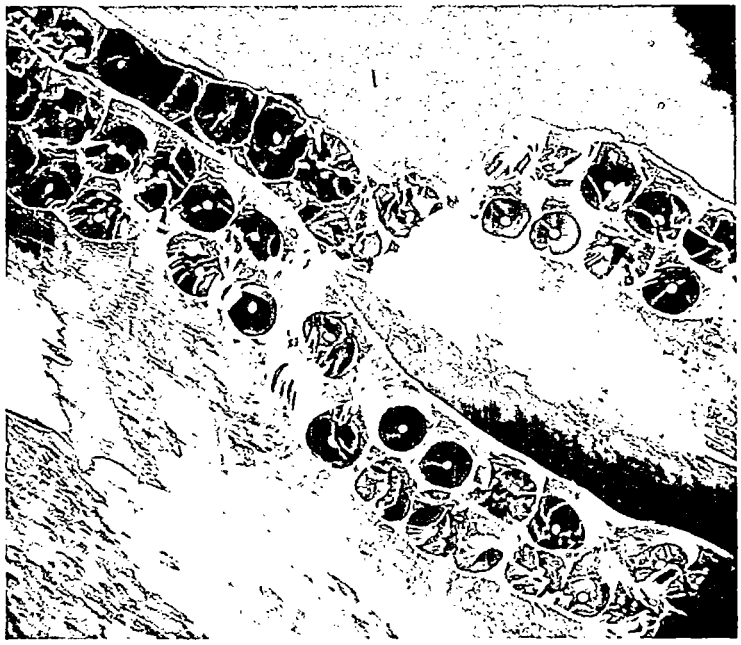

L-72-161

Figure 17.- General view of matching fracture surfaces of bilayer B-Al composite exhibiting axial fracture. Filament diameter, 0.099 mm (0.0039 in.).

L-72-162

Figure 18.- Details of an axial shear surface in bilayer B-Al composite. Filament diameter, 0.099 mm (0.0039 in.).

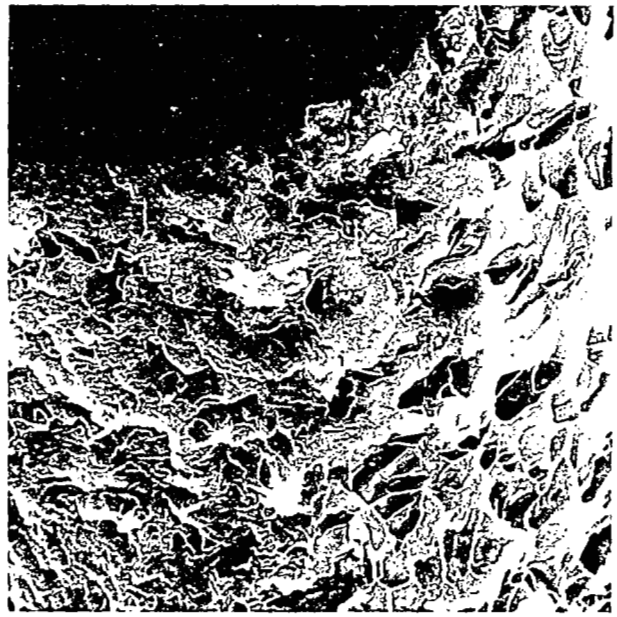

(a) Rupture on side of exposed filament in axial shear surface.

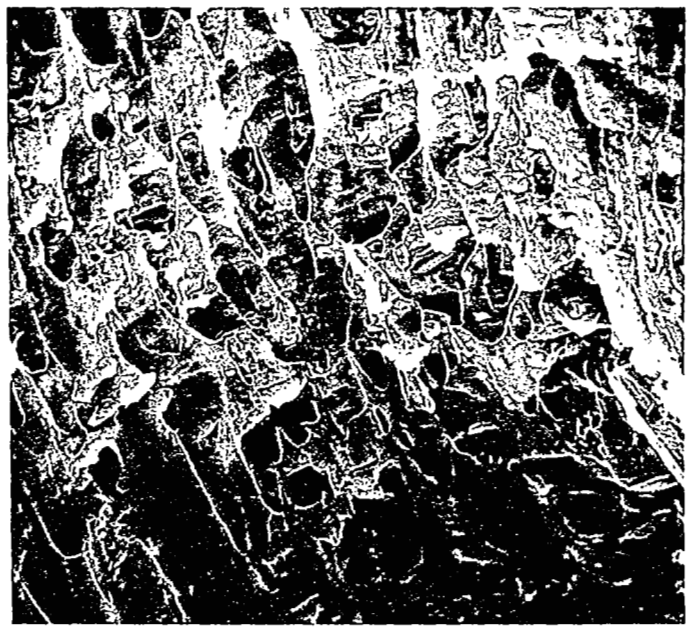

L-72-163

(b) Matching surface from which exposed filament was separated.

Figure 19.- Evidence of shear rupture. Filament diameter, 0.099 mm (0.0039 in.).

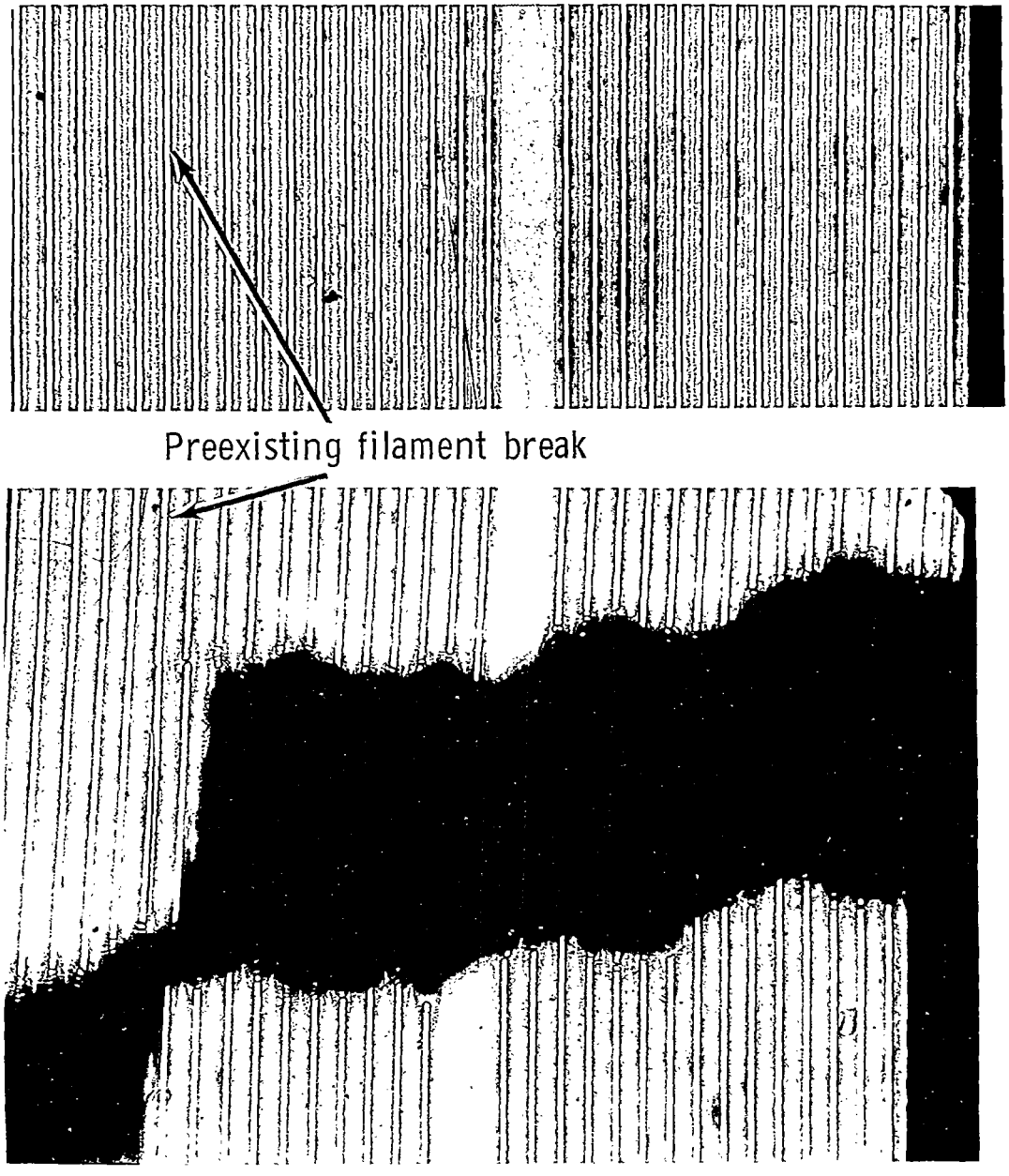

L-72-164

Figure 20.- Fractoradiographs of monolayer B-Al composite showing role of preexisting filament break in promoting development of axial fracture. Core diameter, 0.015 mm (0.0006 in.).

L-72-165

Figure 21.- General view of bilayer B-Al composite fracture surface with split filament in axial portion. Filament diameter, 0.099 mm (0.0039 in.).

L-72-166

Figure 22.- Details of axial fracture surface containing split filament. Filament diameter, 0.099 mm (0.0039 in.).

L-72-167

Figure 23.- Closeup of split filament in axial fracture surface.

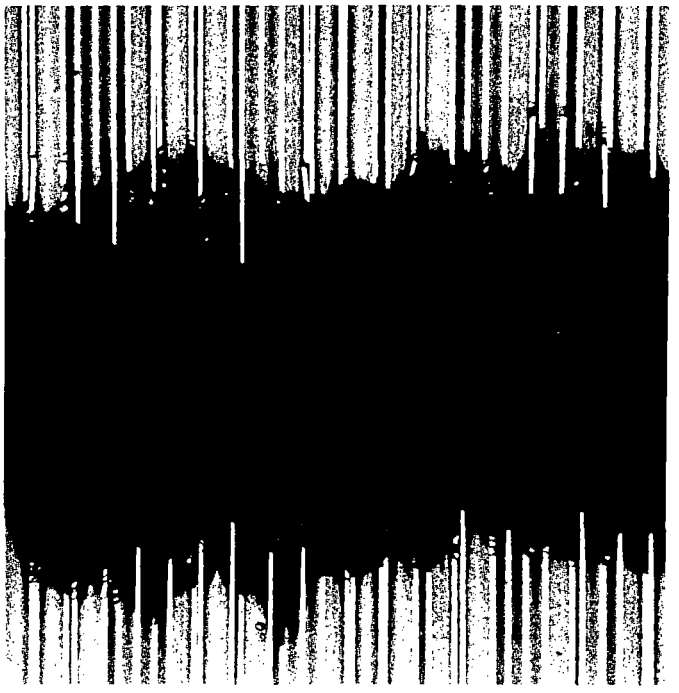

L-72-168

Figure 24.- Fractoradiograph of bilayer B-Al composite exhibiting canted fracture. Core diameter, 0.015 mm (0.0006 in.).

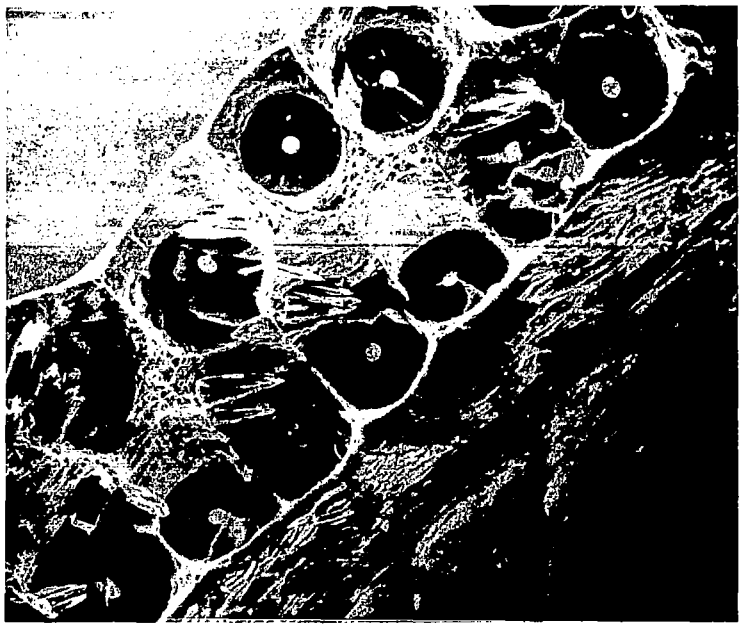

L-72-169

Figure 25. - Details of a canted fracture surface in bilayer B-Al composite. Filament diameter, 0.099 mm (0.0039 in.).

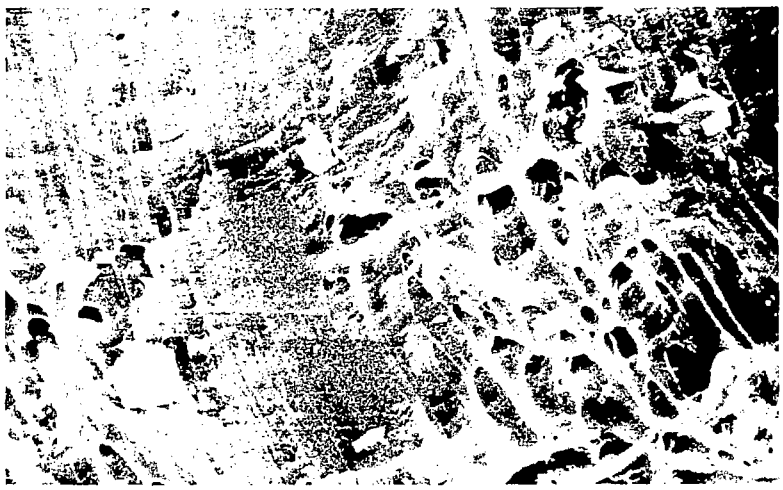

L-72-170

Figure 26. - Details of matrix shear in canted fracture surface.

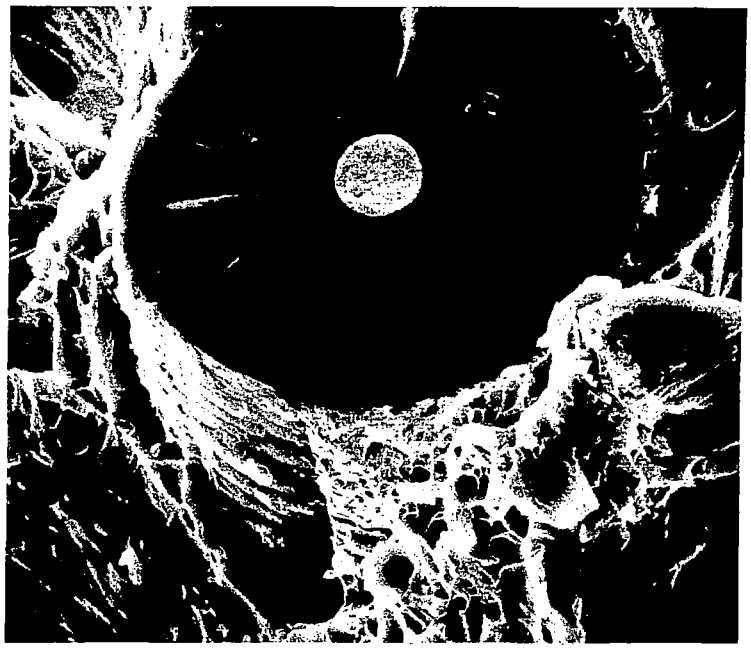

(a) Unbonded strip on side of exposed filament.

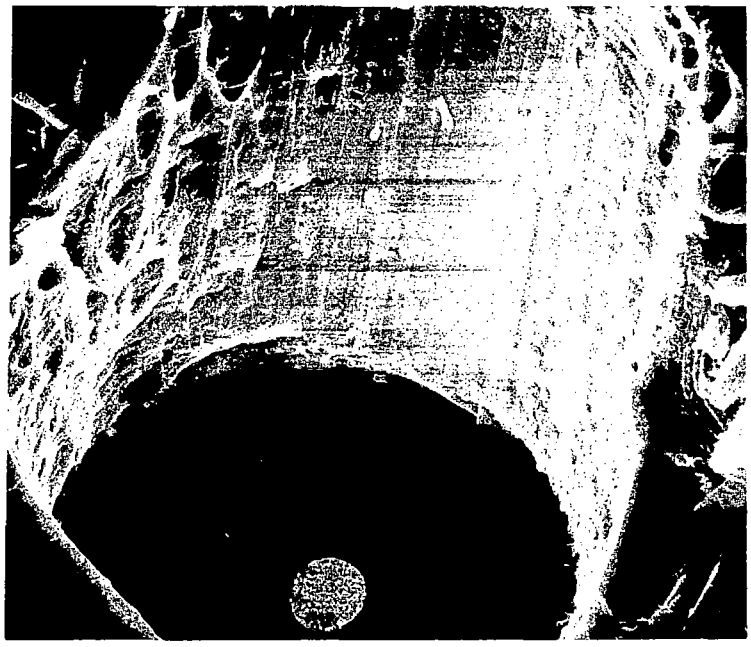

L-72-171

(b) Corresponding unbonded area in mating surface.

Figure 27.- Matching 0.099-mm-diameter (0.0039-in.) filament fracture surfaces in canted fracture region.

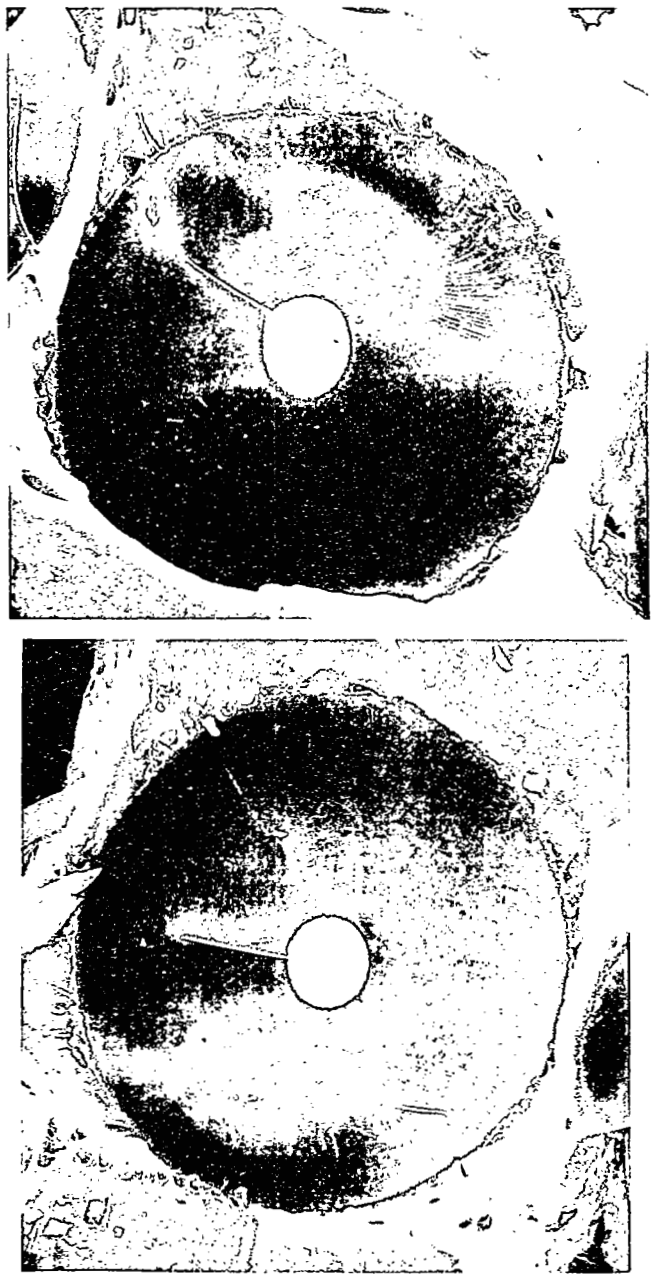

L-72-172

Figure 28.- Matching surfaces of unfragmented 0.099-mm-diameter (0.0039-in.) boron filament from transverse B-Al composite fracture surface.

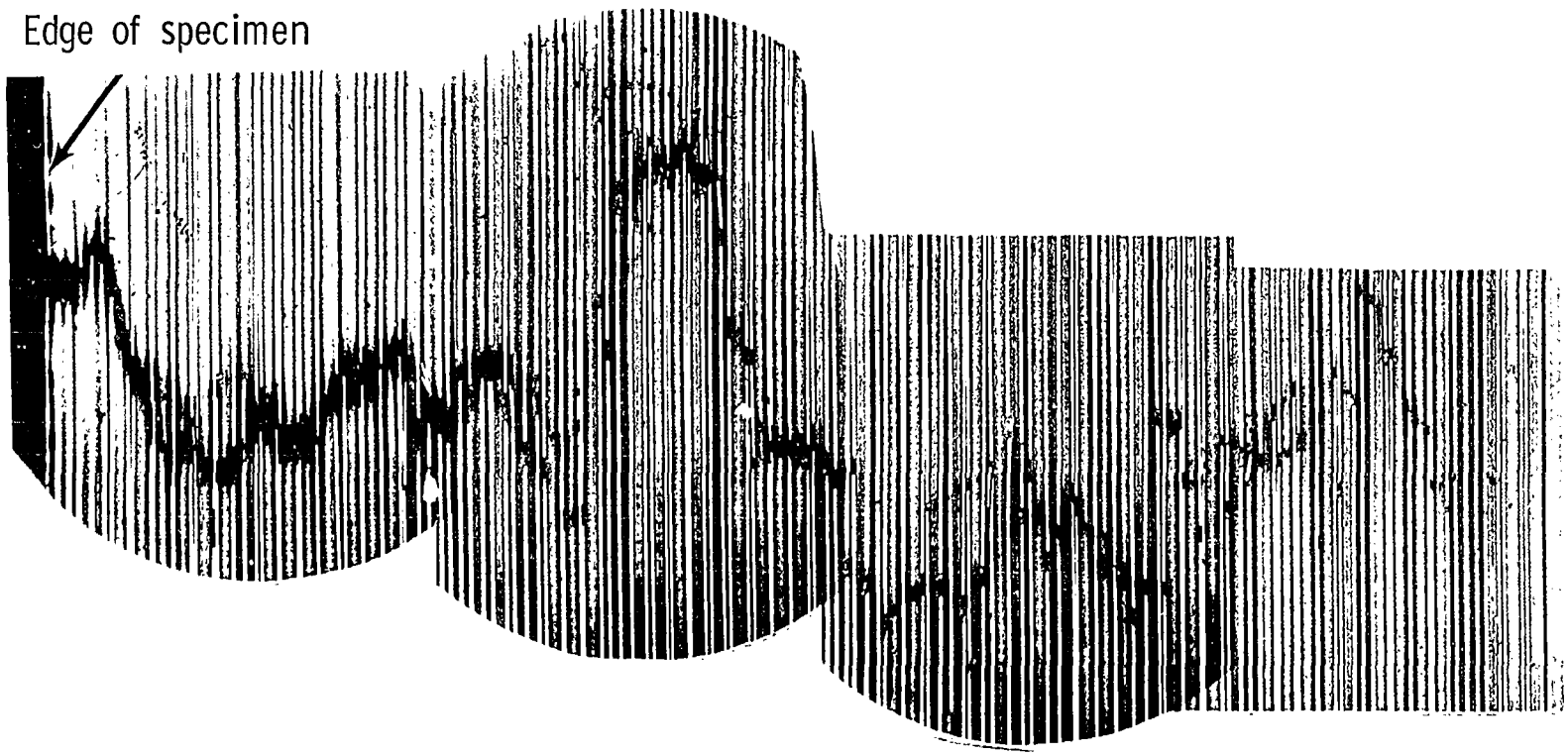

L-72-173

Figure 29.- Fractoradiograph showing arrested cumulative crack in bilayer B-Al composite. Core diameter, 0.015 mm (0.0006 in.).

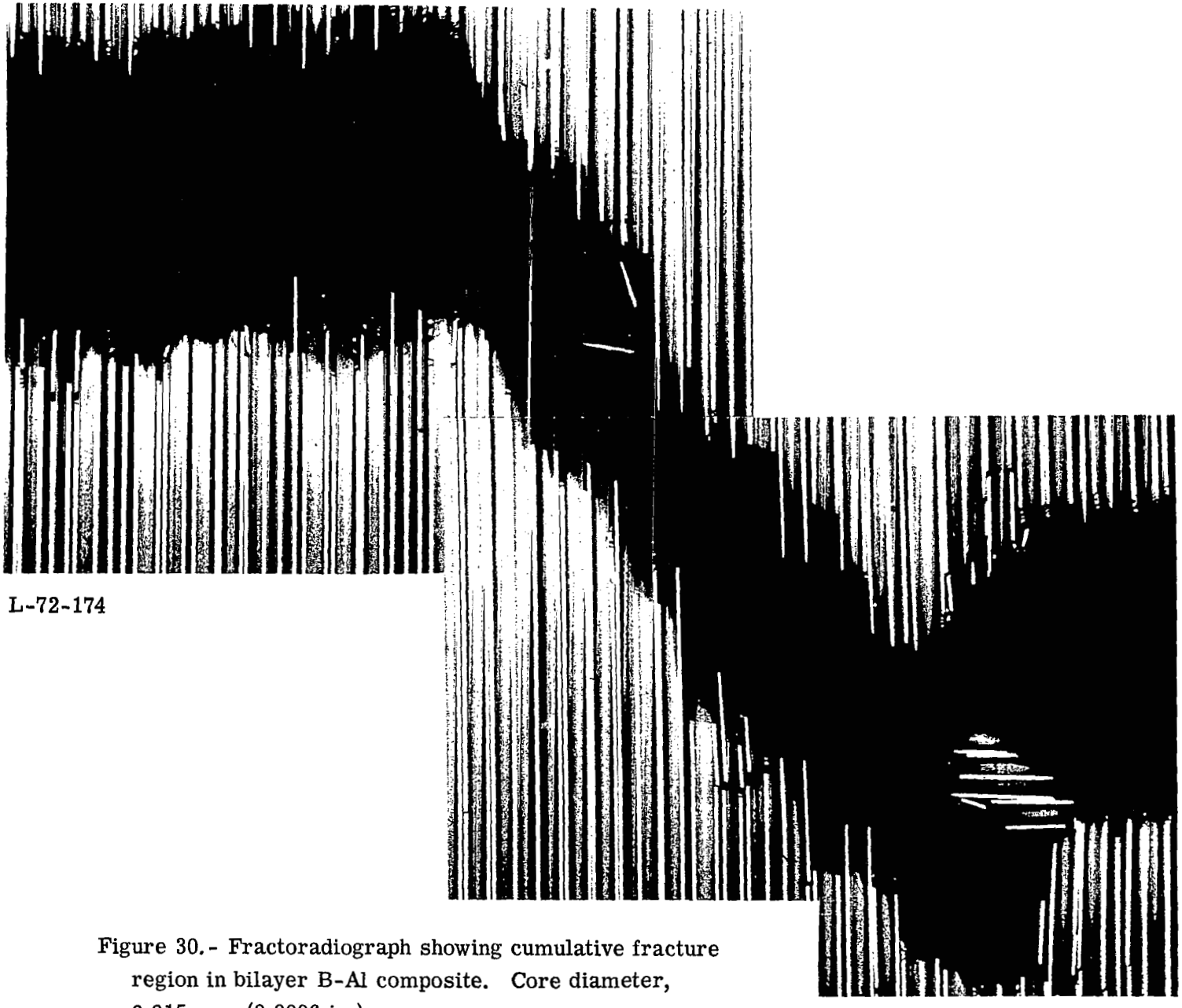

L-72-174

Figure 30.- Fractoradiograph showing cumulative fracture region in bilayer B-Al composite. Core diameter, 0.015 mm (0.0006 in.).

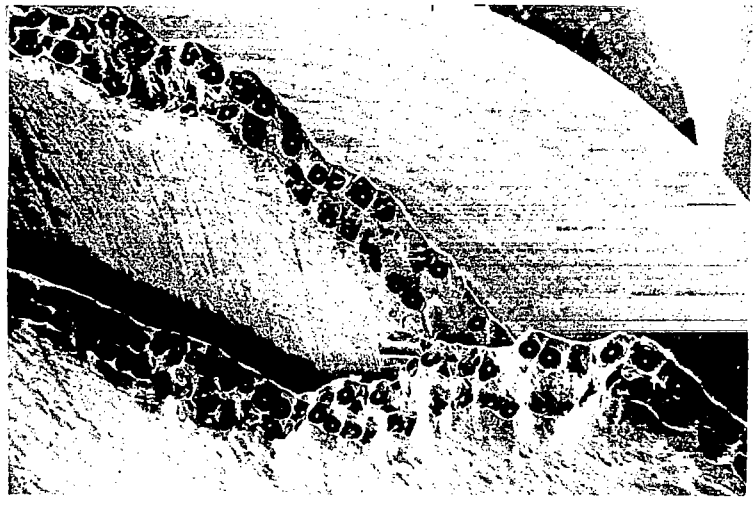

L-72-175

Figure 31.- General view of cumulative region in matching bilayer B-Al composite fracture surfaces. Filament diameter, 0.099 mm (0.0039 in.).

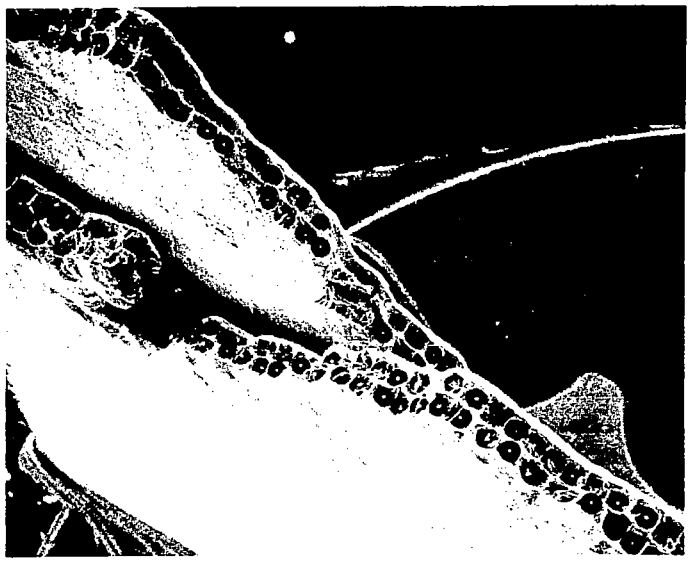

L-72-176

Figure 32.- Same surface as in figure 31, but rotated to show surface hidden in figure 31.

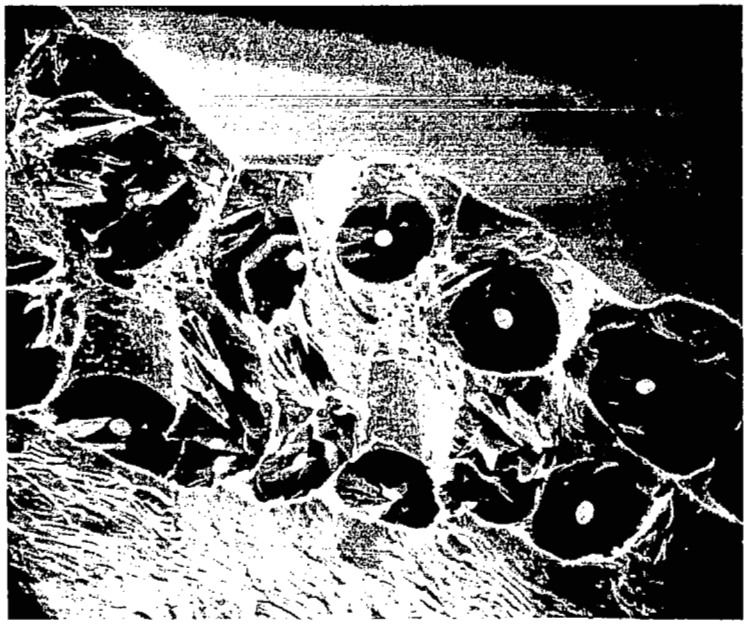

L-72-177

Figure 33.- Details of a canted fracture surface associated with partially cumulative fracture in bilayer B-Al composite. Filament diameter, 0.099 mm (0.0039 in.).

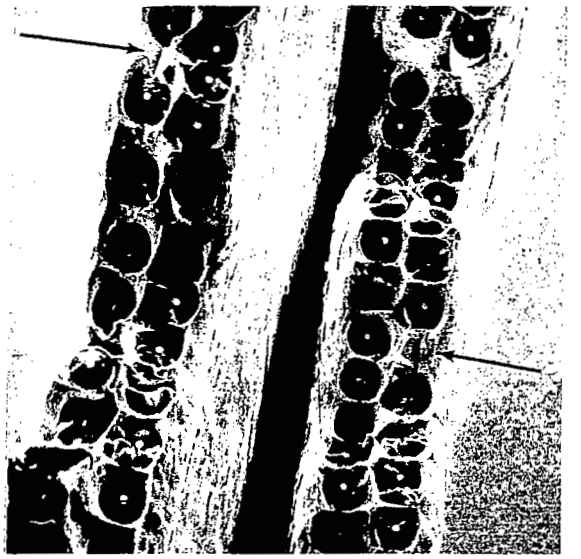

L-72-178

Figure 34.- General view of matching fracture surfaces in bilayer B-Al composite with weak internal bonding. Filament diameter, 0.089 mm (0.0035 in.).

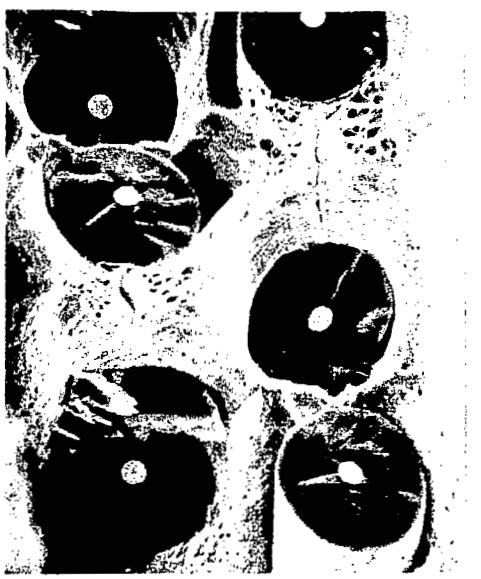

L-72-179

Figure 35.- Debonding around broken filaments in fracture surface of B-Al composite with weak internal bonding. Filament diameter, 0.089 mm (0.0035 in.).

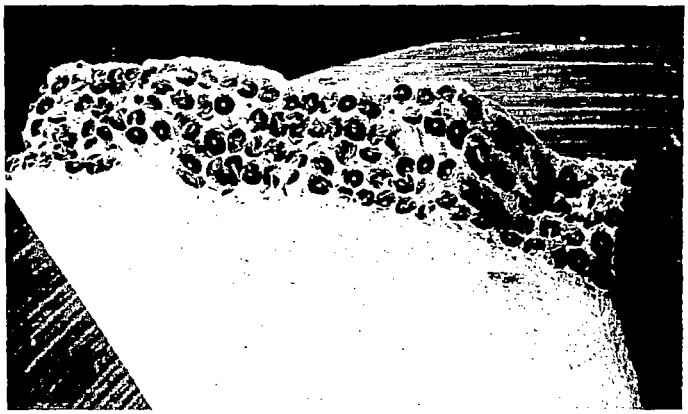

L-72-180

Figure 36.- General view of fracture surface commercially fabricated five-layer composite. Filament diameter, 0.10 mm (0.0041 in.).

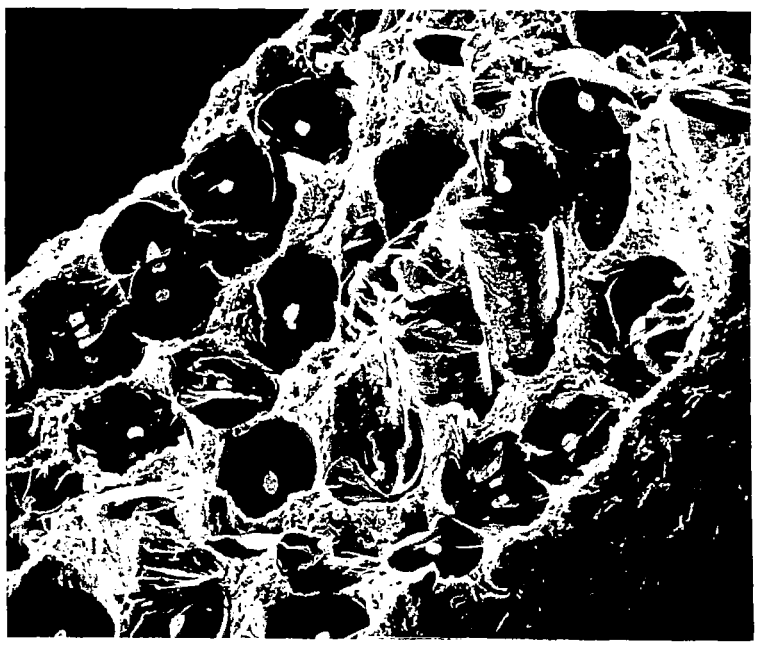

L-72-181

Figure 37.- Leftmost transition region between transverse noncumulative and cumulative fracture in fracture surface of figure 36.

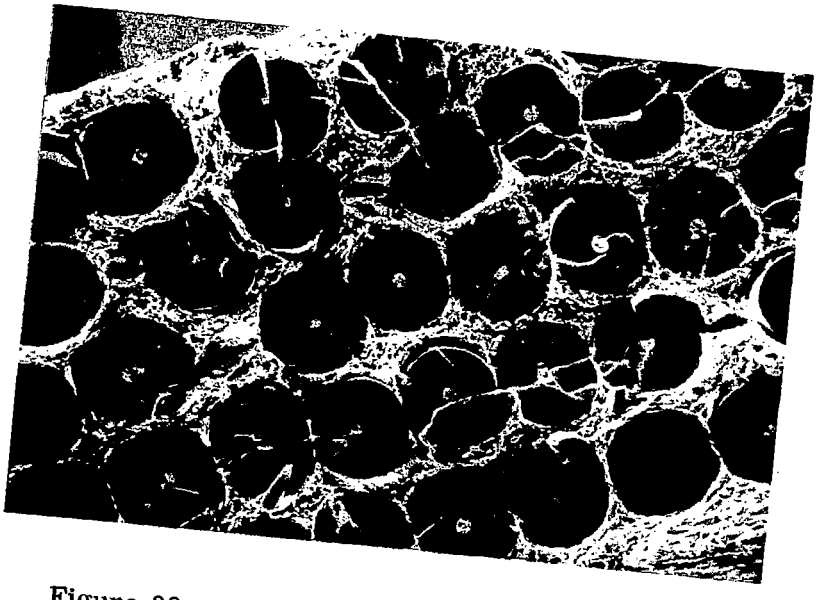

Figure 38.- Second transverse region from left edge of fracture surface of figure 36. L-72-182

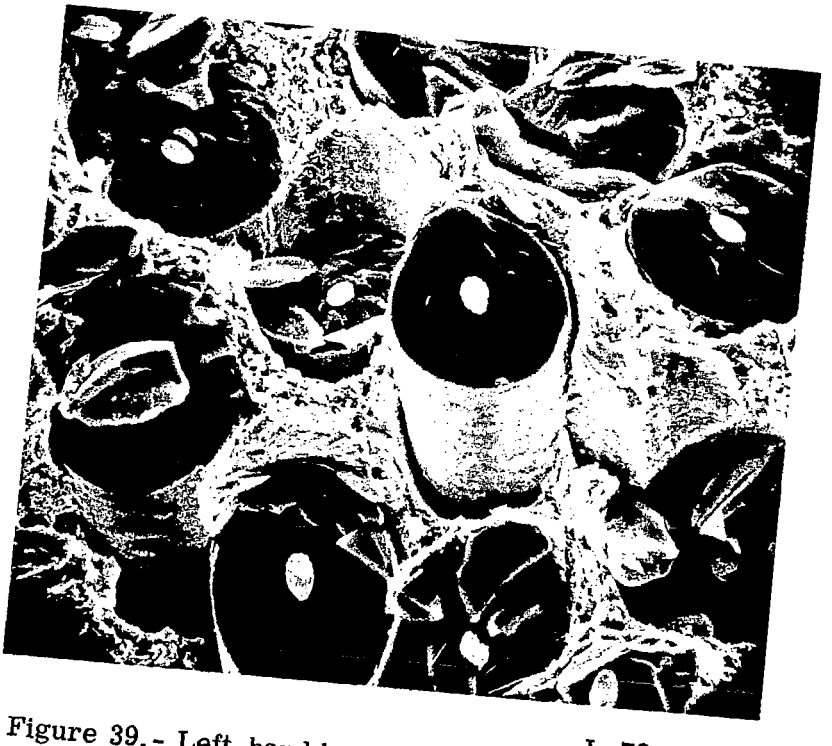

Figure 39.- Left-hand boundary of second transverse region of figure 36. L-72-183

L-72-184

Figure 40.- General view of transverse noncumulative fracture surface in commercially fabricated monolayer composite. Filament diameter, 0.14 mm (0.0056 in.).

L-72-185

Figure 41.- Typical case of axial fracture in commercially fabricated monolayer composite. Filament diameter, 0.14 mm (0.0056 in.).

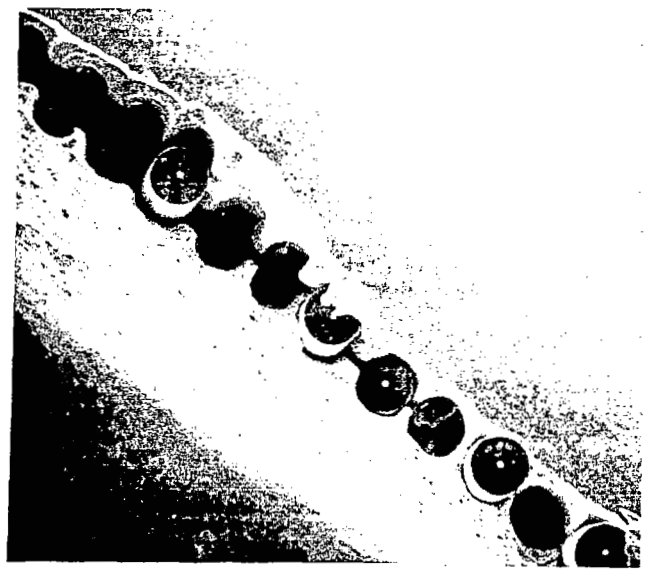

L-72-186

Figure 42.- Delamination in extremely weakly bonded region of commercially fabricated monolayer composite. Filament diameter, 0.14 mm (0.0056 in.).

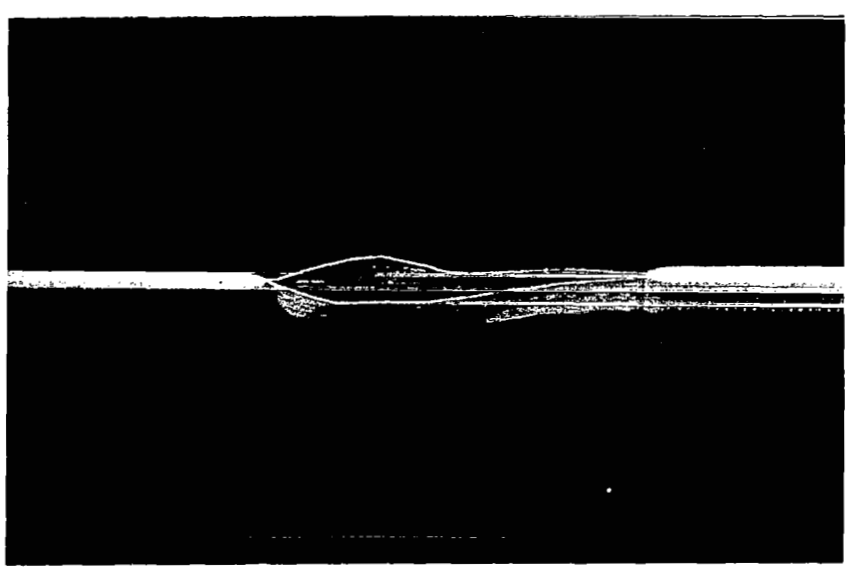

L-72-187

Figure 43.- Gross delamination of extremely weakly bonded specimen of commercially fabricated monolayer composite. Filament diameter, 0.14 mm (0.0056 in.).

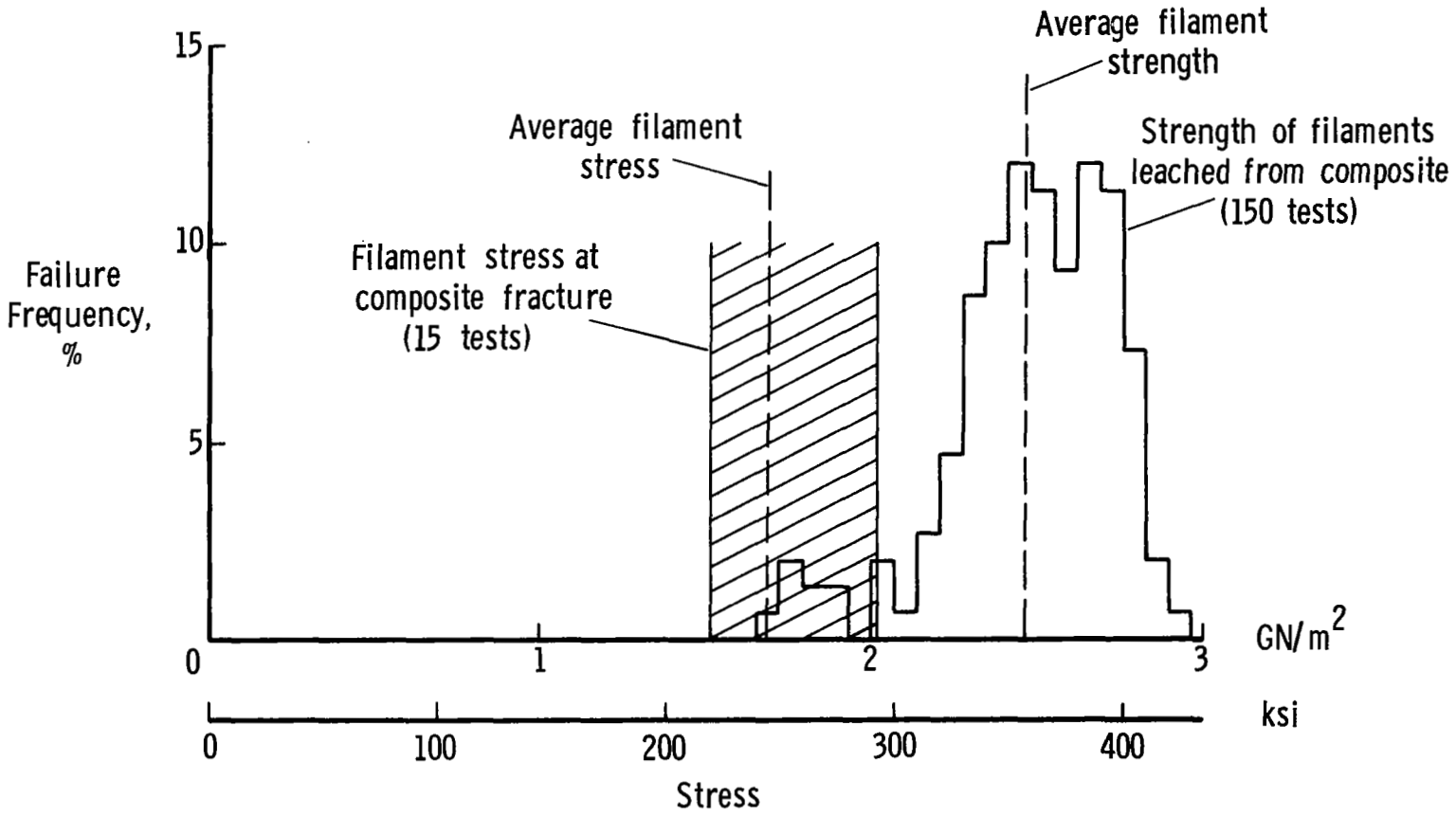

Figure 44.- Average filament stress at composite fracture and filament strength in composite for monolayer sheet containing 0.14-mm-diameter (0.0056-in.) boron filaments. Consolidated under pressure of 69 MN/m^2 (10 ksi) at 866 K (1100° F).

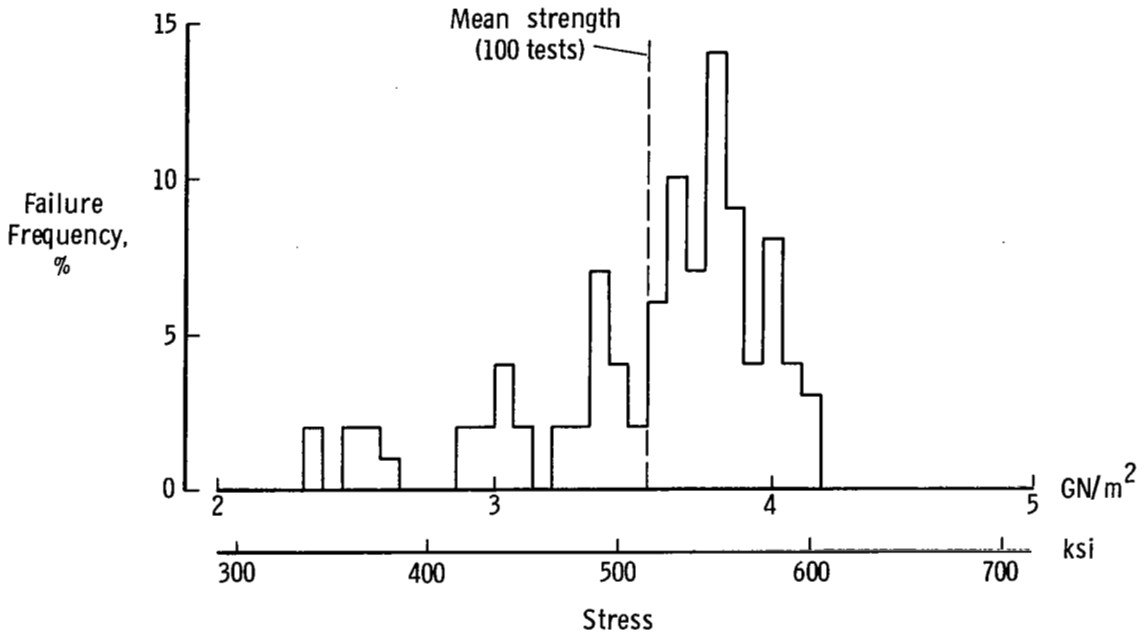

Figure 45.- Failure-frequency histogram for virgin 0.14-mm-diameter (0.0056-in.) boron filament.

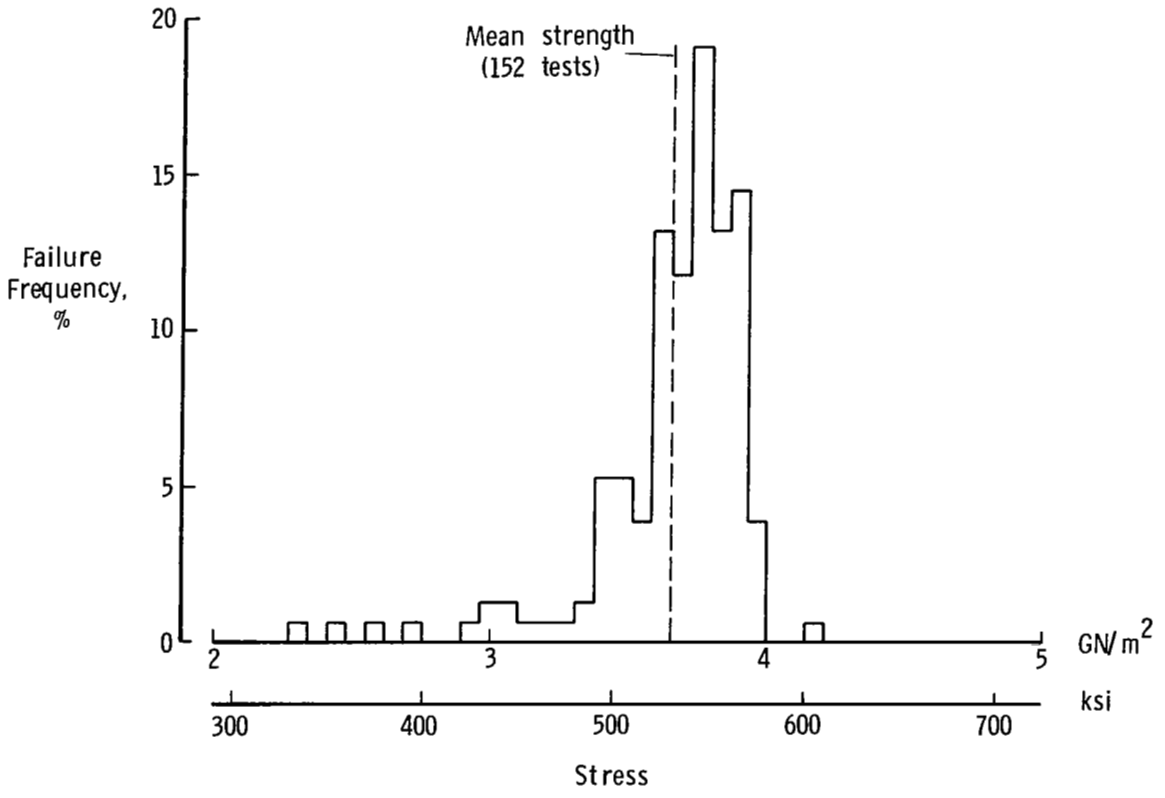

Figure 46.- Failure-frequency histogram for virgin 0.099-mm-diameter (0.0039-in.) boron filament.

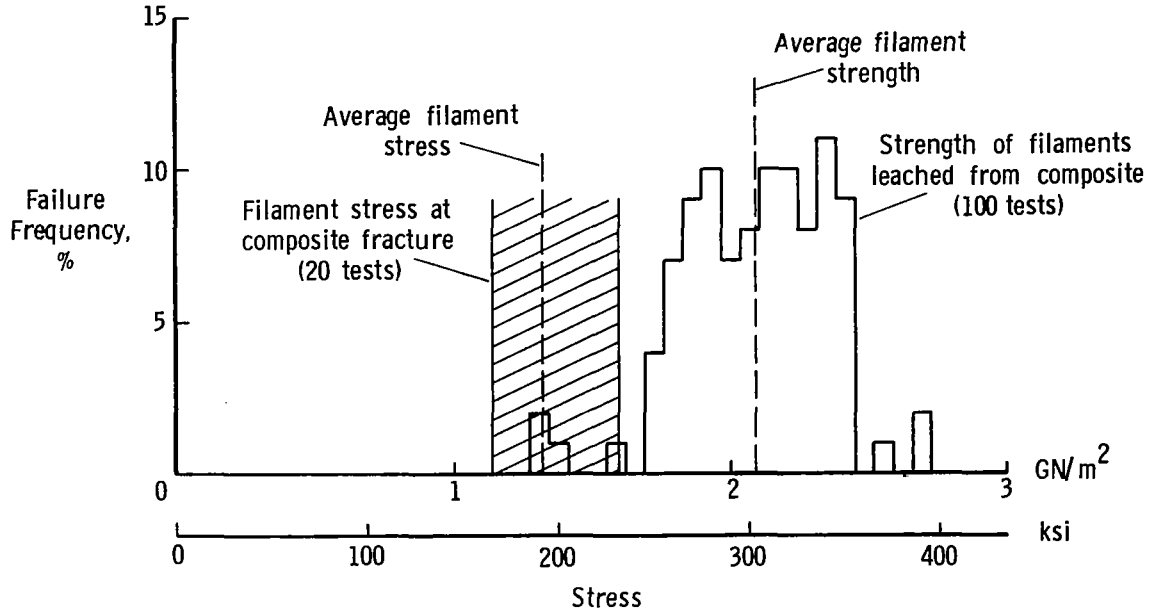

(a) Consolidated under pressure of 69 MN/m^2 (10 ksi) at 866 K (1100° F).

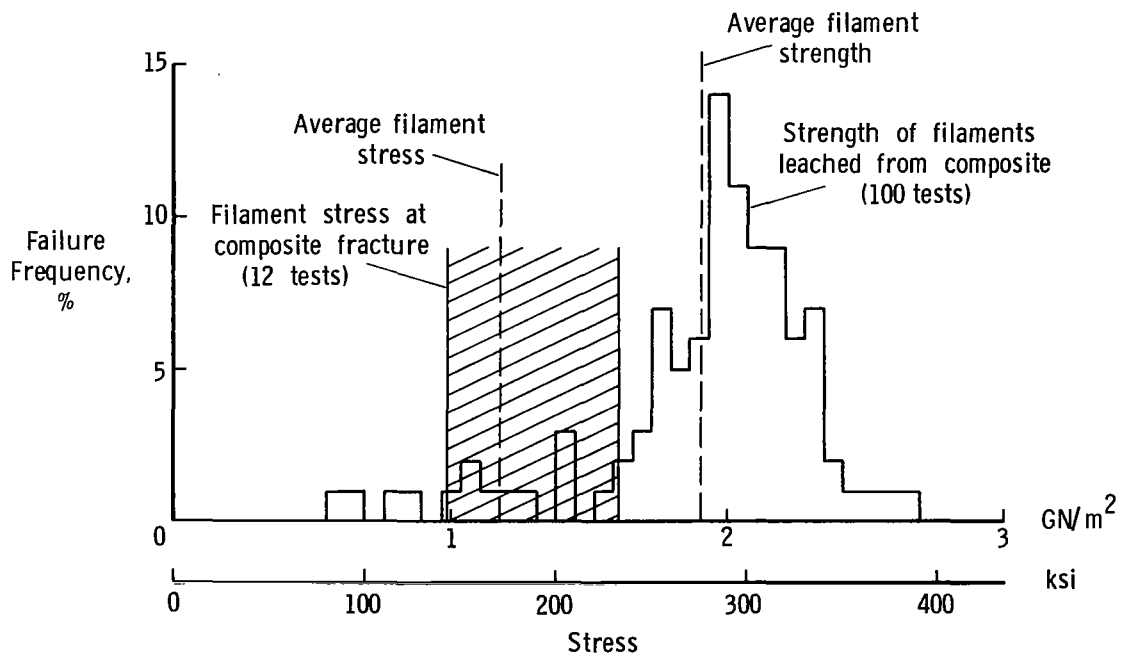

(b) Consolidated under pressure of 76 MN/m^2 (11 ksi) at 866 K (1100° F).

Figure 47.- Average filament stress at composite fracture and filament strength in composite for bilayer sheet containing 0.099-mm-diameter (0.0039-in.) boron filaments.

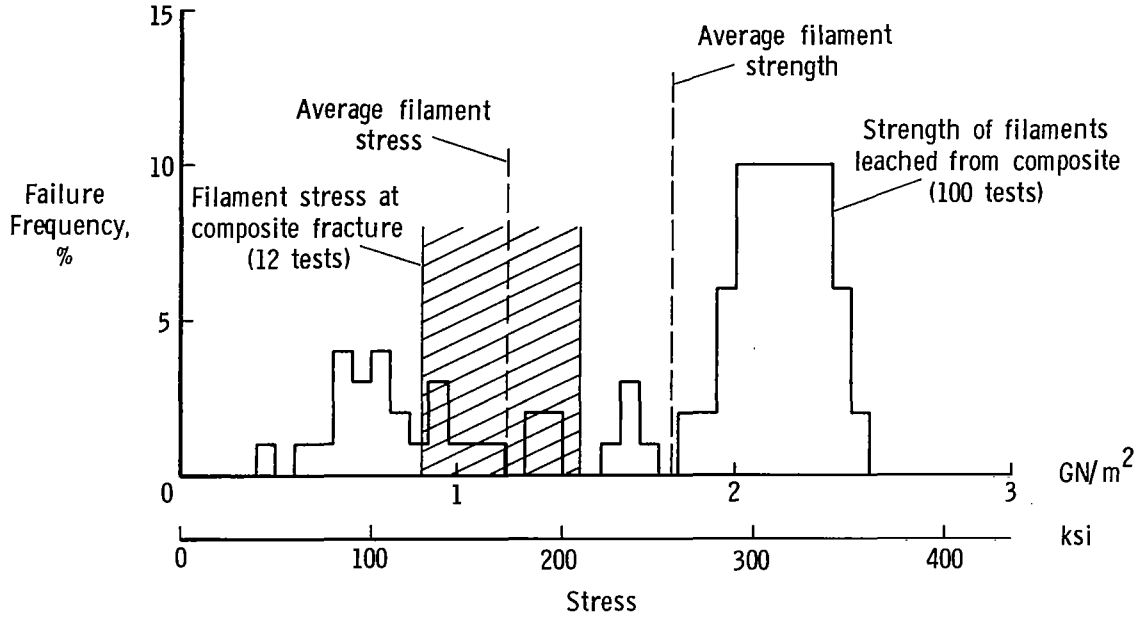

(c) Consolidated under pressure of 83 MN/m^2 (12 ksi) at 866 K (1100° F).

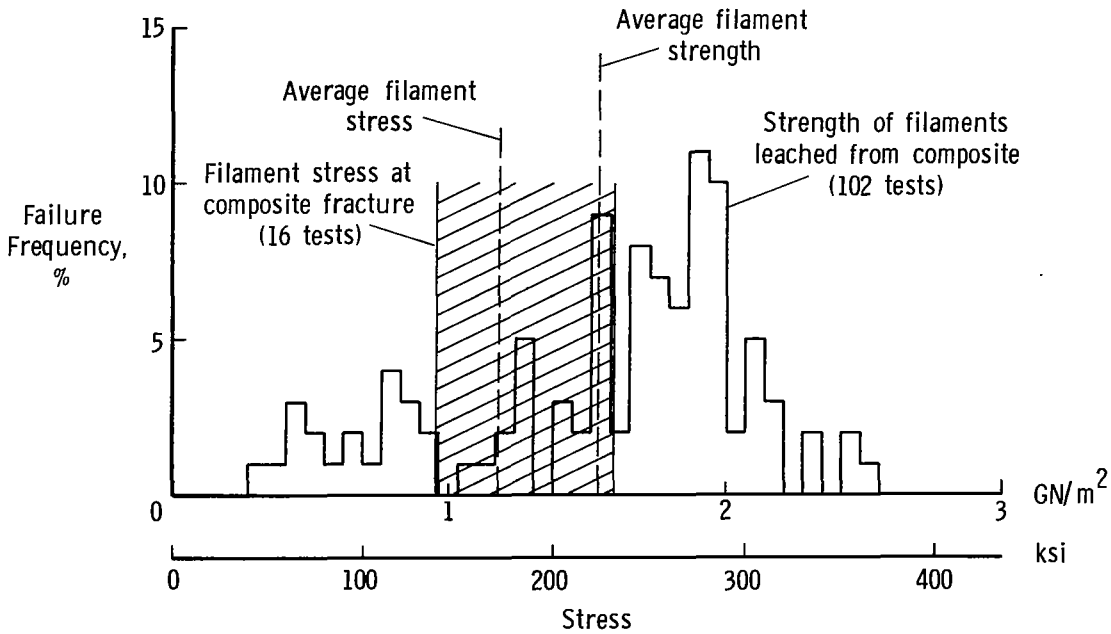

(d) Consolidated under pressure of 90 MN/m^2 (13 ksi) at 866 K (1100° F).

Figure 47.- Continued.

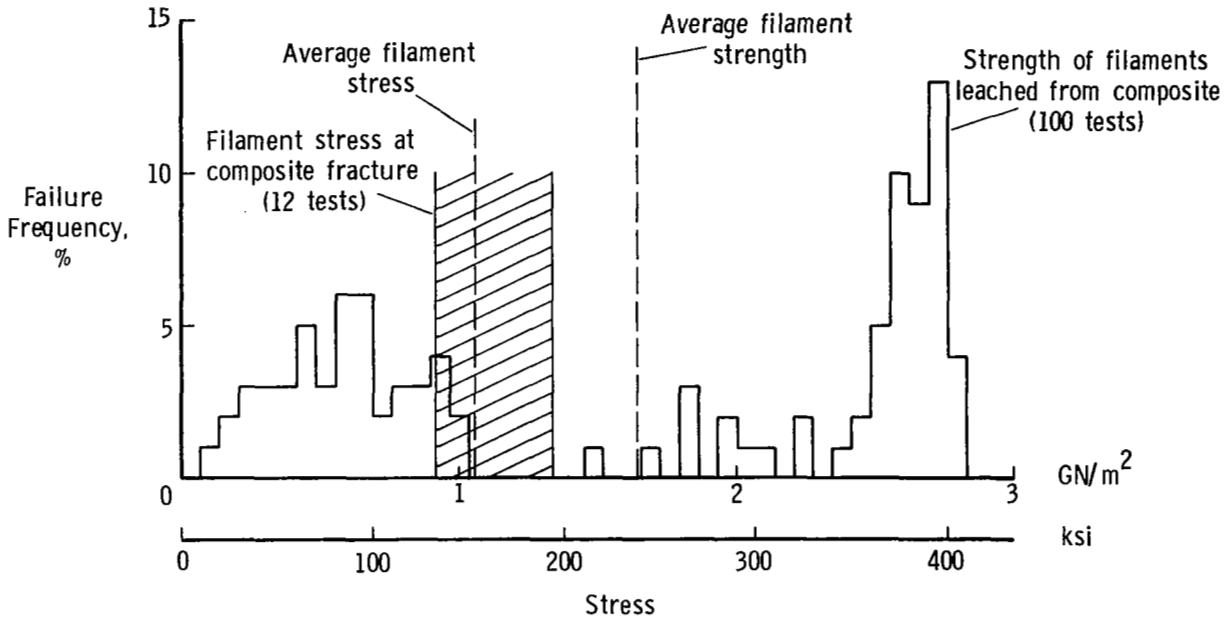

(e) Consolidated under pressure of 103 MN/m^2 (15 ksi) at 866 K (1100° F).

Figure 47.- Concluded.

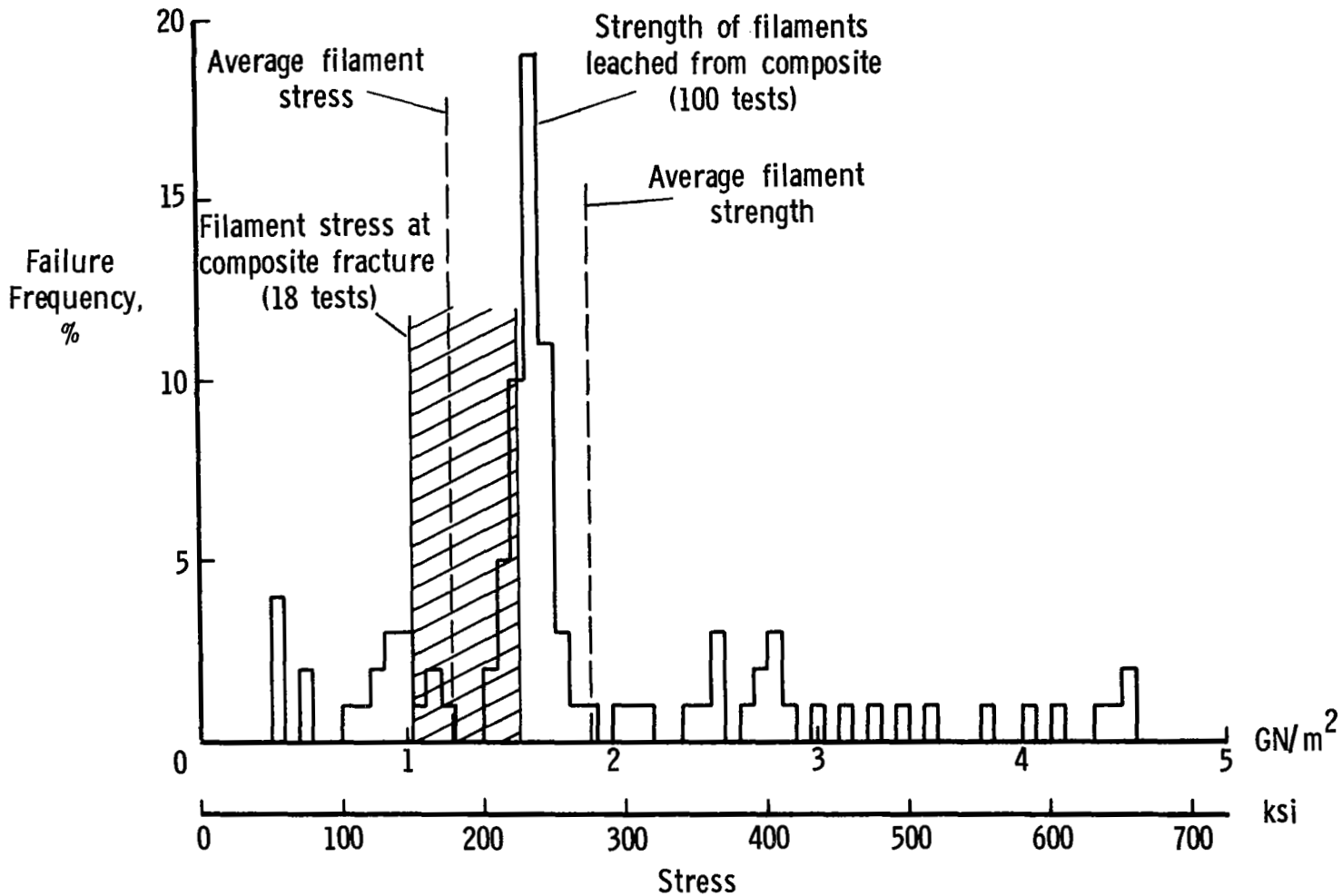

Figure 48.- Average filament stress at composite fracture and filament strength in composite for bilayer sheet containing 0.089-mm-diameter (0.0035-in.) boron filaments. Consolidated under pressure of 62 MN/m^2 (9 ksi) at 783 K (950° F).

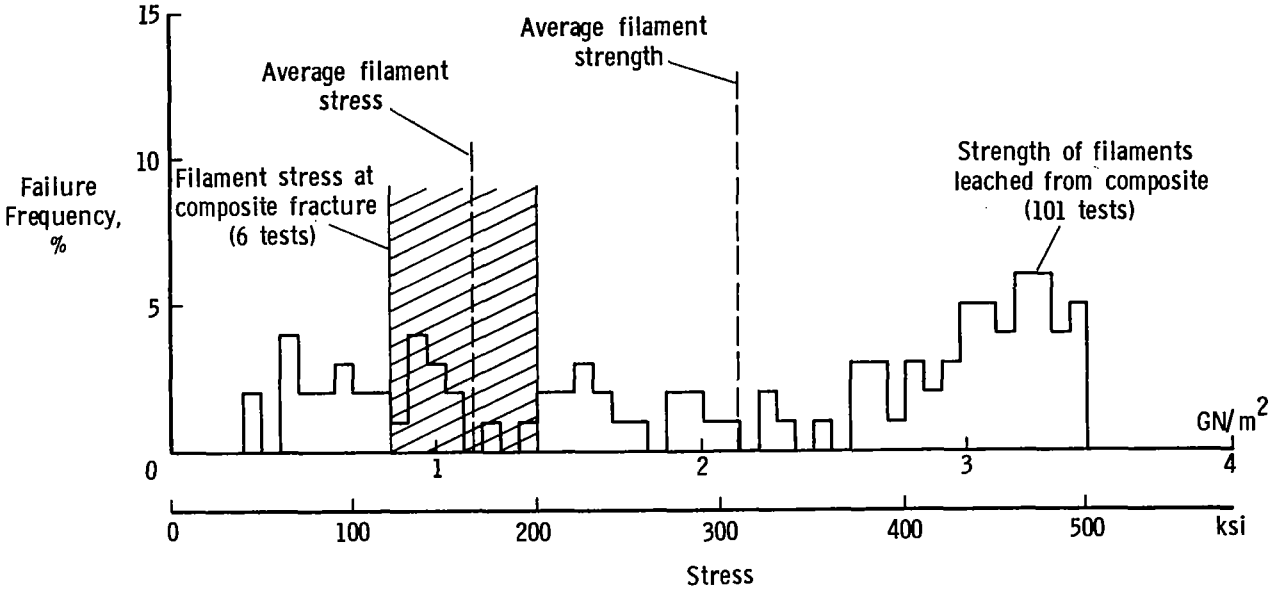

Figure 49.- Average filament stress at composite fracture and filament strength in composite for commercially fabricated five-layer sheet containing 0.10-mm-diameter (0.0041-in.) silicon-carbide-coated boron filaments.

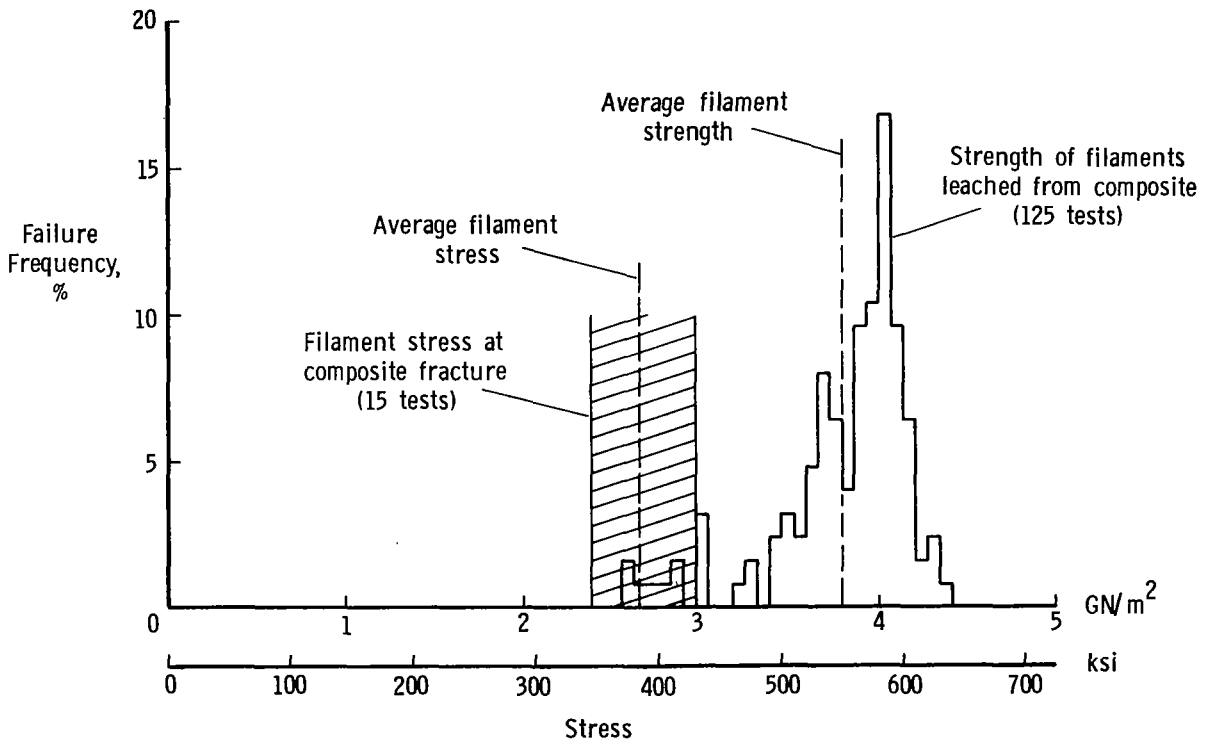

Figure 50.- Average filament stress at composite fracture and filament strength in composite for commercially fabricated monolayer sheet containing 0.14-mm-diameter (0.0056-in.) boron filaments.

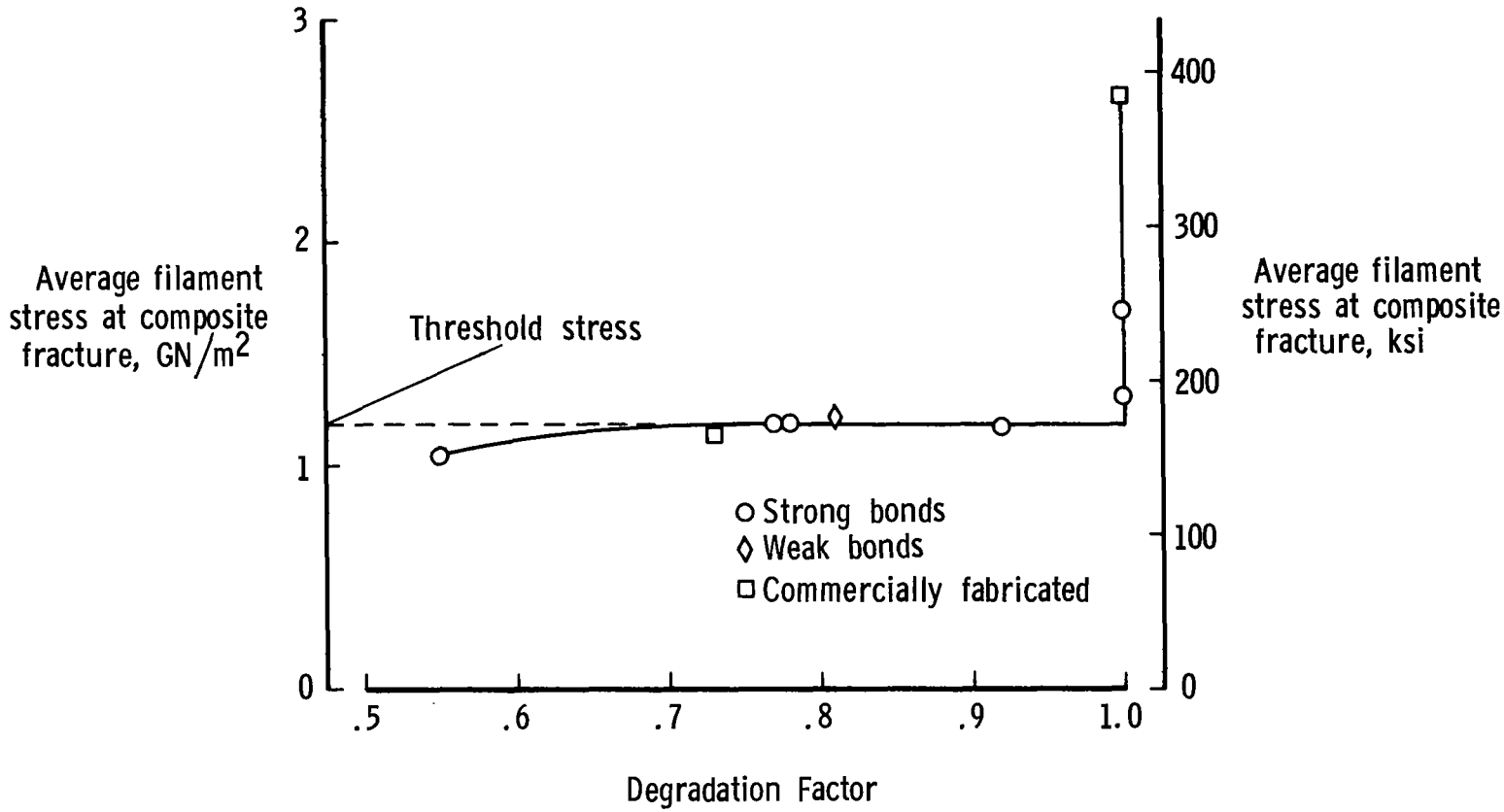

Figure 51.- Threshold stress for initiation and sustenance of noncumulative filament-break propagation in unidirectional B-Al composite sheet.

L-72-188

Figure 52.- Radiograph through gage section of monolayer B-Al composite tensile specimen containing four damaged filaments. Core diameter, 0.015 mm (0.0006 in.).

L-72-189

Figure 53.- Radiograph through gage section of monolayer B-Al composite tensile specimen containing 14 damaged filaments. Core diameter, 0.015 mm (0.0006 in.).

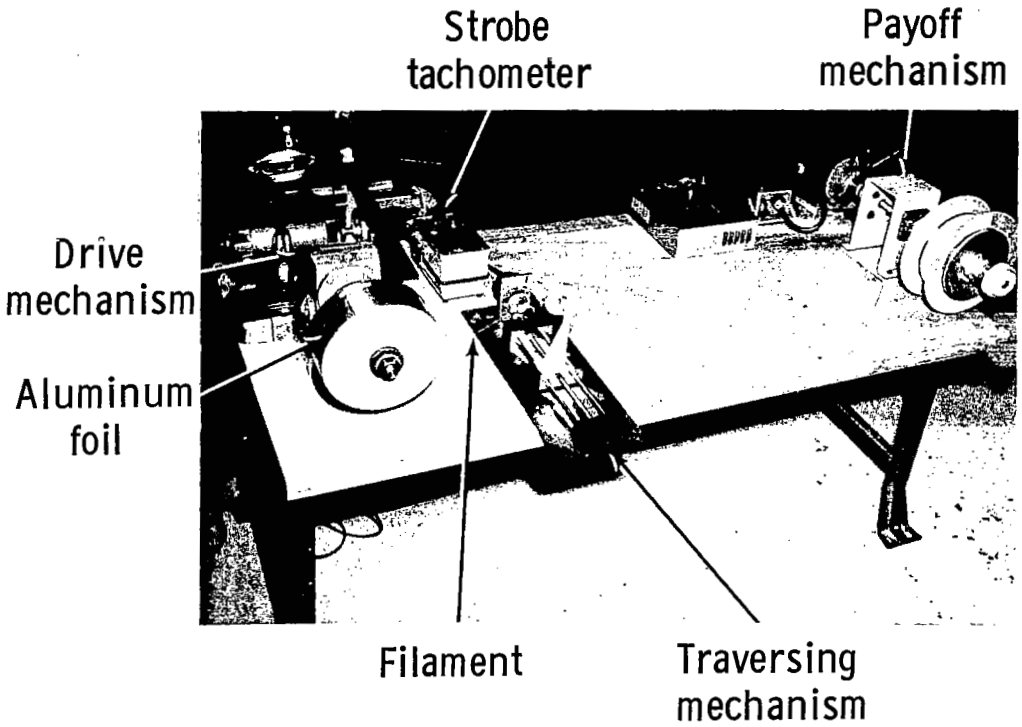

L-72-190

Figure 54.- Filament-winding apparatus used in fabrication of B-Al composite sheet.

NASA-Langley, 1972 —— 17 L-8137

NATIONAL AERONAUTICS AND SPACE ADMISTRATION
WASHINGTON, D.C. 20546

OFFICIAL BUSINESS
PENALTY FOR PRIVATE USE $300

FIRST CLASS MAIL

POSTAGE AND FEES PAID
NATIONAL AERONAUTICS AND
SPACE ADMINISTRATION

U.S.MAIL

021 001 C1 U 17 720414 S00903DS
DEPT OF THE AIR FORCE
AF WEAPONS LAB (AFSC)
TECH LIBRARY/WLOL/
ATTN: E LOU BOWMAN, CHIEF
KIRTLAND AFB NM 87117

POSTMASTER: If Undeliverable (Section 15
Postal Manual) Do Not Retu

"The aeronautical and space activities of the United States shall be conducted so as to contribute . . . to the expansion of human knowledge of phenomena in the atmosphere and space. The Administration shall provide for the widest practicable and appropriate dissemination of information concerning its activities and the results thereof."

— NATIONAL AERONAUTICS AND SPACE ACT OF 1958

NASA SCIENTIFIC AND TECHNICAL PUBLICATIONS

TECHNICAL REPORTS: Scientific and technical information considered important, complete, and a lasting contribution to existing knowledge.

TECHNICAL NOTES: Information less broad in scope but nevertheless of importance as a contribution to existing knowledge.

TECHNICAL MEMORANDUMS: Information receiving limited distribution because of preliminary data, security classification, or other reasons.

CONTRACTOR REPORTS: Scientific and technical information generated under a NASA contract or grant and considered an important contribution to existing knowledge.

TECHNICAL TRANSLATIONS: Information published in a foreign language considered to merit NASA distribution in English.

SPECIAL PUBLICATIONS: Information derived from or of value to NASA activities. Publications include conference proceedings, monographs, data compilations, handbooks, sourcebooks, and special bibliographies.

TECHNOLOGY UTILIZATION PUBLICATIONS: Information on technology used by NASA that may be of particular interest in commercial and other non-aerospace applications. Publications include Tech Briefs, Technology Utilization Reports and Technology Surveys.

Details on the availability of these publications may be obtained from:

SCIENTIFIC AND TECHNICAL INFORMATION OFFICE

NATIONAL AERONAUTICS AND SPACE ADMINISTRATION

Washington, D.C. 20546